

Review

Recent progress in metal-organic frameworks-based hydrogels and aerogels and their applications

Luyu Wang^a, Hui Xu^b, Junkuo Gao^{a,*}, Juming Yao^{a,*}, Qichun Zhang^{c,*}^a Institute of Fiber Based New Energy Materials, The Key Laboratory of Advanced Textile Materials and Manufacturing Technology of Ministry of Education, School of Materials Science and Engineering, Zhejiang Sci-Tech University, Hangzhou 310018, China^b College of Materials Science and Engineering, China Jiliang University, Hangzhou 310018, China^c School of Materials Science & Engineering, Nanyang Technological University, Singapore 639798, Singapore

ARTICLE INFO

Article history:

Received 15 June 2019

Accepted 23 July 2019

Available online 6 August 2019

Keywords:

Metal-organic frameworks

Hydrogels

Aerogels

Application

ABSTRACT

In recent years, metal-organic frameworks (MOFs) have attracted incredible chemical and material research interests because of their prominent properties and charming structures. The reliable production of a wide variety of MOFs materials and MOF derivatives, such as MOF-metal nanoparticles composites and MOFs-polymers hybrids, offers many possibilities to develop MOF-based applied materials. Although MOFs have many unique features, including abundant pore structures and multiple functional ligands, their applied performance is limited by intrinsic fragility and powdered crystalline state, as well as unsatisfied stability and processability. By this, MOF-based hydrogels and aerogels have achieved unparalleled results, outperforming ungelated MOFs materials in many aspects. This review presents current developments of MOF-based hydrogels and aerogels with emphasis on the specific categories and the synergistic effects of MOF-derived aerogels between MOFs and additional materials. Particular emphasis is placed on discussing the advantages of MOF-based hydrogels and aerogels in applications such as sensors, batteries, supercapacitors, adsorbents, catalysts etc. MOF-based hydrogels and aerogels can provide valuable guidance for the investigation of MOFs towards practical applications with processability, stability, and easy handling. Specifically, we will summary recent progress of pure MOF hydrogels, MOF@biology derived organic macromolecules hydrogels, MOF@biocompatible hydrogels, MOF@ graphene hydrogels, pure MOF aerogels, MOF@silica aerogel composites, MOF@ graphene aerogel composites, MOF@cellulose aerogel composites, and aerogel composites containing MOFs-derived materials. In addition, their applications are also discussed. We hope that this review will be helpful for those who want quick access to valuable references about MOF-based hydrogels and aerogels and their applications.

© 2019 Elsevier B.V. All rights reserved.

Contents

1. Introduction	2
2. The methods for synthesis of MOF-based hydrogels and aerogels	4
2.1. Direct mixing method	4
2.2. <i>In situ</i> MOF synthesis	4
3. The categories of MOF-based hydrogels and aerogels	4
3.1. MOF-based hydrogels	4
3.1.1. Pure MOF hydrogels	5
3.1.2. MOF@biology derived organic macromolecules hydrogels	5
3.1.3. MOF@biocompatible hydrogels	7
3.1.4. MOF@graphene hydrogels	7
3.2. MOF-based aerogels	8

* Corresponding authors at: Institute of Fiber Based New Energy Materials, The Key Laboratory of Advanced Textile Materials and Manufacturing Technology of Ministry of Education, School of Materials Science and Engineering, Zhejiang Sci-Tech University, Hangzhou 310018, China (J. Gao, J. Yao) and School of Materials Science & Engineering, Nanyang Technological University, Singapore 639798, Singapore (Q. Zhang).

E-mail addresses: jkgao@zstu.edu.cn (J. Gao), yaoj@zstu.edu.cn (J. Yao), qc Zhang@ntu.edu.sg (Q. Zhang).

3.2.1.	Pure MOF aerogels	9
3.2.2.	MOF@silica aerogel composites	10
3.2.3.	MOF@graphene aerogel composites	10
3.2.4.	MOF@cellulose aerogel composites	11
3.2.5.	MOF@organic polymers aerogel composites	12
3.2.6.	Aerogel composites containing MOFs-derived materials	12
3.2.7.	Other aerogel composites	13
4.	The applications of MOF-based hydrogels and aerogels	14
4.1.	MOF-based hydrogels	14
4.1.1.	Drug release	14
4.1.2.	Wound healing	16
4.1.3.	Sensing	16
4.1.4.	Water treatment	17
4.2.	MOF-based aerogels	17
4.2.1.	Energy storage	18
4.2.2.	Catalysis	20
4.2.3.	Water treatment	22
4.2.4.	Gas adsorption	24
4.2.5.	Sensing	25
5.	Conclusions and outlook	25
	Acknowledgements	26
	References	26

1. Introduction

The research of metal-organic frameworks (MOFs), also known as porous coordination polymers, is growing very fast [1–6]. This upsurge can be reflected in the increasing number of papers published over the last fifteen years, as shown in Fig. 1a. As special porous crystalline materials, MOFs are formed by the linkage between organic ligands and metal-containing nodes through coordination bonds [7–9]. Up to now, tens of thousands of MOFs with various molecular compositions, topologies, crystal structures, pore structures, and surface morphologies have been discovered because of these diverse metal nodes and ligands [10–15]. In addition, many MOF composites have been developed and are active in various applications [16–18]. The tunability of MOFs is based on their multitudinous composition, physical properties, topology of the underlying nets, ligands, and metal nodes. By using some rational methods such as interweaving motif, mixed-ligand strategy and functionalization, etc., the properties and application performance of MOFs can be tuned [19–22]. The tunability of MOFs paves the way for their applications, such as molecular separation, energy storage, catalysis, gas adsorption, luminescent sensing, and drug delivery, etc [23–32]. However, some practical applications are hindered by the disadvantageous nature of MOFs, such as rigidity and very easy to be crumbled. Besides, MOFs with high crystallinity always show intrinsic fragility and unsatisfied processability [33]. Although MOFs in crystalline powder states have rich pore

structures, most of them are micropores, which will result to poor surface accessibility [34]. Therefore, designing flexible and stable MOF-based materials with good surface accessibility, flexible processability and high surface area is a meaningful strategy for improving the practical performances of MOFs.

Given the tunable multifunction, small size, and microporous structure, the use of MOFs as a functional reinforcing additive agent for inactive chemical composites has attracted significant interest [35]. However, the high activity of MOFs and their tendency to decomposition in hydrophilic media, have made the efficient utilization of these MOFs-based composites very challenging. In response to this problem, several waterproof MOFs have been reported to improve stability [36–38]. This high activity of MOFs is beneficial in their use as reinforcing additive agents of hydrogels. Hydrogels are generally considered as highly hydrated cross-linked three-dimensional (3D) networks that contain a wide range of structural forms and chemical compositions [39]. The increasing number of the related reports (Fig. 1b) indicates the popularity of hydrogels. The 3D networks can be used to promote the dispersibility of MOFs in hydrogel matrices. Conversely, MOFs can interact with other components or tune the properties of hydrogel matrices. Particularly, tailoring the chemical properties of hydrogels remains a barrier to the successful translation of hydrogels to specific applications, which is important to create high applied performance functional materials. Moreover, the metal-ion stability of some MOFs in hydrogel matrices makes them attractive in

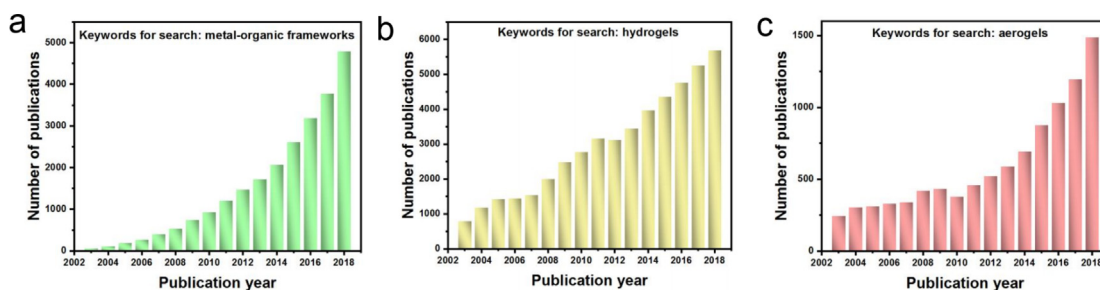


Fig. 1. (a) The number of publications in the area of MOFs from 2003 to 2018 (internet search of the Scopus on May 27, 2019). Keywords for search: metal-organic frameworks. (b) The number of publications in the area of hydrogels from 2003 to 2018 (internet search of the Scopus on July 14, 2019). Keywords for search: hydrogels. (c) The number of publications in the area of aerogels from 2003 to 2018 (internet search of the Scopus on July 14, 2019). Keywords for search: aerogels.

biological applications such as drug delivery and wound healing. All of these applications are served by high porosity, water content, and cytocompatibility of hydrogels.

However, in practical application fields such as adsorption and catalysis, the network structure of materials is required to be free of liquid. By some special drying methods such as critical point drying and freeze-drying, the liquid in the macro-scale gels can be removed. The corresponding product is called aerogel. Aerogel possesses a space network structure filled with gas [40]. Aerogels are lightweight nanoporous materials that have continuous 3D nanoporous network structure composed of nanoparticles, and they are endowed with unique structural characteristics such as low density, high porosity, high specific surface area, and large pore volume, etc [41]. These advantages enable aerogels to have good performances in thermal insulation, gas adsorption, water treatment, catalysis and so on [42], and make the research of aerogels more and more attractive, as shown in Fig. 1c. The first aerogel in the world was prepared using supercritical drying technology in 1931 by Kistler, which replaced the liquid component in the gel with gases and kept the gel wall from collapsing [43]. According to Kistler, aerogels should possess the following characteristics: (1) the aerogels are obtained via drying the hydrogels; (2) the aerogels have no obvious shrinkage and fragmentation of hydrogels during drying process; (3) typical aerogels have complete crack-free appearance; and (4) The aerogels possess high porosity [44]. According to the types of matrix, aerogels can be divided into oxide aerogels, carbide aerogels, organic aerogels, carbon aerogels, etc. The classical preparation of aerogels consists of two processes: sol-gel process and drying process. The former process mainly obtains gels with certain space network structures while the latter one aims to remove the solvents from the network of the gels and obtain the final aerogels. In addition, in order to meet the requirement of applications, the preparation of aerogels also currently needs additional auxiliary processes, including aging, surface modification, solvent replacement, and thermal treatment, etc [45]. Comparing with other aerogels, MOFs-based aerogels possess enhanced mechanical properties (due to the rigid structure of MOFs) and high specific surface areas (due to the microporous structure of MOFs).

The various processing methods for the preparation of MOF-based hydrogels and aerogels have also increased the wide application of these materials. Hydrogels are mainly prepared by adding

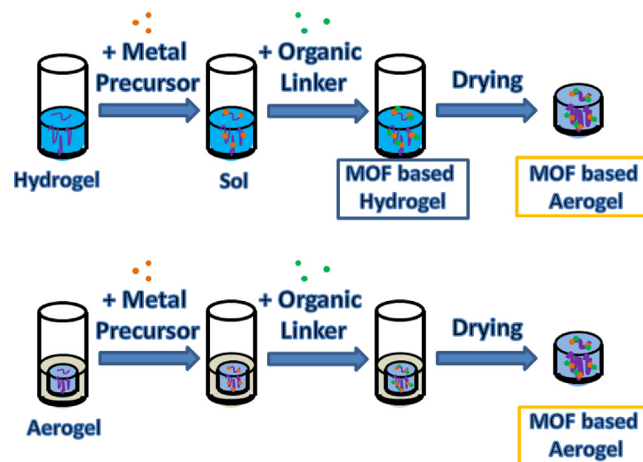


Fig. 3. The preparation processes of MOF-based hydrogels and aerogels *in situ* on hydrogels and aerogels.

MOFs to a polymer precursor solution. Then, the chemically crosslinking of the polymer components that surround the MOFs can be realized by free radical polymerization. On the other hand, aerogels can be prepared by using the method of freeze-drying or critical point drying to treat a precursor material or gel. The aqueous gel phase is replaced by gas (air) to form a solid or supercritical regime [46]. As a result, the MOF-based hydrogels and aerogels can take into account the advantages of both MOFs and hydrogels/aerogels. In addition, there are many kinds of MOFs and hydrogels and aerogels, which provide a wide space for the development of composite materials. It is reasonable to believe that the advantages from both two components (MOFs and hydrogels/aerogels) can be retained while some shortcomings from two components can be avoided. Such composites can achieve optimized performance, which can upgrade their application areas.

Considering the superiority of MOF-based hydrogels and aerogels, this review will try to provide a comprehensive overview of the MOF-based hydrogels and aerogels that have been reported until now, including pure MOF hydrogels, MOF@biology derived organic macromolecules hydrogels, MOF@biocompatible hydrogels, MOF@ graphene hydrogels, pure MOF aerogels, MOF@silica

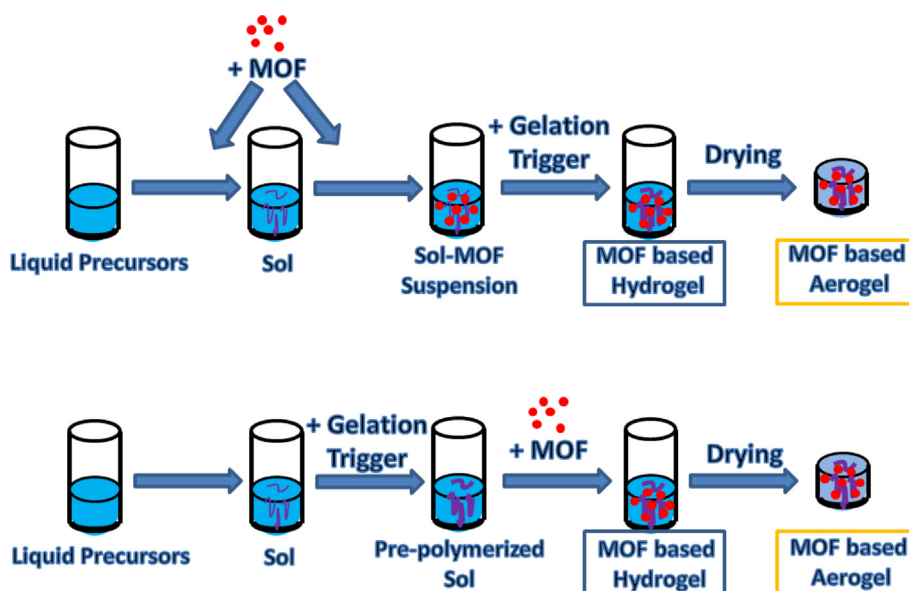


Fig. 2. The preparation processes of MOF-based hydrogels and aerogels by using the direct mixing method.

Table 1
The Summary of MOF-based hydrogels.

MOF	Matrix	Application	Ref
Eu-MOFs, Tb-MOFs, and Dy-MOFs	–	tunable emission and multi-target detection	[49]
ZIF-8	gelatin hydrogel	–	[50]
HKUST-1	gelatin hydrogel	–	[50]
ZIF-8	poly (vinylalcohol)-chitosan hydrogel	CO ₂ capture	[51]
UiO-66-NH ₂	agarose hydrogel	sensing	[52]
HKUST-1	alginate hydrogel	water treatment	[53]
ZIF-8	alginate hydrogel	water treatment	[53]
MIL-100(Fe)	alginate hydrogel	water treatment	[53]
ZIF-67	alginate hydrogel	water treatment	[53]
copper-vitamin MOF	alginate hydrogel	wound healing	[54]
Zinc-vitamin MOF	alginate hydrogel	wound healing	[54]
zeolite-like MOF	N-vinyl-2-pyrrolidinone hydrogel	Drug release	[55]
UiO-68	polyacrylamide/DNA hydrogel	Drug release	[56]
HKUST-1	PPCN hydrogel	wound healing	[57]
Zinc-MOF	GO hydrogel	–	[58]
ZIF-8	Graphene hydrogel	biomass degradation	[59]
ZIF-8	laponite clay hydrogel	–	[60]
HKUST-1	PVA-co-PE/PVA hybrid hydrogel	adsorption	[61]
MOF [Eu ₂ (BPDC)(BDC) ₂ (H ₂ O) ₂] _n	alginate hydrogel	Sensing	[62]
Co-MOF	alginate hydrogel	water treatment	[63]
ZIF-8	polyacrylamide hydrogel	water treatment	[64]

aerogel composites, MOF@ graphene aerogel composites, MOF@-cellulose aerogel composites, and aerogel composites containing MOFs-derived materials, because the variety of MOFs affords a huge number of possible combinations. Herein, the categories of MOF-based hydrogels and aerogels have been introduced firstly. Then, their existing applications are discussed. We hope that this carefully-prepared review will inspire the skilled chemists in other fields to investigate more MOF materials beyond powder MOFs, and bring inexperienced researchers into more practical applications based on MOF-based hydrogels and aerogels.

2. The methods for synthesis of MOF-based hydrogels and aerogels

MOF-based hydrogels and aerogels are generally synthesized by incorporating MOFs into the hydrogel or aerogel matrixes. Correspondingly, the MOFs can be considered as the dispersed phase, meanwhile, the hydrogel or aerogel matrixes are the continuous phase. MOF-based hydrogels and aerogels can be shaped into various structures. MOF-based hydrogels and aerogels can be synthesized via using the following two different methods: (1) Direct mixing method and (2) *In situ* MOF synthesis. For aerogels, the final drying step is added.

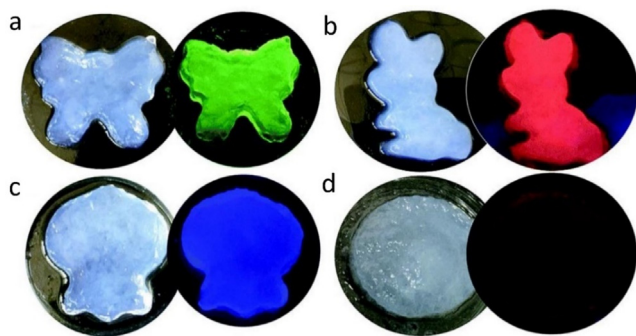


Fig. 4. Photographs of (a) Tb-Dy MOF hydrogel, (b) Eu-Tb MOF hydrogel, (c) Eu-Dy MOF hydrogel, and (d) Eu-Tb-Dy MOF hydrogel with mixed-metal ratios of 1:1 or 1:1:1 under sunlight (left) and under excitation at 275 nm (right). Reproduced with permission [49]. Copyright 2019 Published by The Royal Society of Chemistry.

2.1. Direct mixing method

In this method, before gelation, the procedures for hydrogels are modified by adding MOF crystals to the liquid precursor or the sol, as shown in Fig. 2. The final gelation of the hydrogel matrixes entraps the MOF crystals to produce MOF-based hydrogels. Besides, by using further supercritical drying or freeze-drying methods, MOF-based aerogels can be obtained.

2.2. *In situ* MOF synthesis

Another method for preparing MOF-based hydrogels and aerogels is to *in situ* prepare MOFs inside the pores of hydrogels or aerogels. For aerogels, the final drying step is required. The pores of the hydrogels or aerogels are the bottles while the MOF crystals are the ships. Scientists can make MOFs grow inside the pores of hydrogels or aerogels by sequential adding the metal precursor and the organic linker, as shown in Fig. 3. For synthesis in hydrogels, the precursors of MOFs are incorporated into the hydrogels, and then, the MOF crystals are grown *in situ* inside the pores of the hydrogels to obtain MOF-based hydrogels. The corresponding MOF-based aerogels can be obtained by the drying method. For synthesis in aerogels, the pre-synthesized aerogels are immersed in the solutions of MOF precursors to prepare the MOF crystals inside the pores of the pre-synthesized aerogels, and followed by drying to obtain MOF-based aerogels.

3. The categories of MOF-based hydrogels and aerogels

3.1. MOF-based hydrogels

MOFs composed of metal ions linked by multidentate ligands have attracted significant attention in recent years by the virtue of their potential applications [47]. Overall, the MOFs synthesized by researchers are almost obtained in a powdered crystalline state. The powdered crystalline state limits the industrial applicability of MOFs due to the technical challenges of powders such as poor handling and mass transfer limitations. At the same time, adding MOF powder is beneficial to enhance the mechanical properties of hydrogels [48]. In view of this, MOF-based hydrogels, a new kind of gels, were designed to provide an access to meet the industrial demand. We summarized MOF-based hydrogels in Table 1.

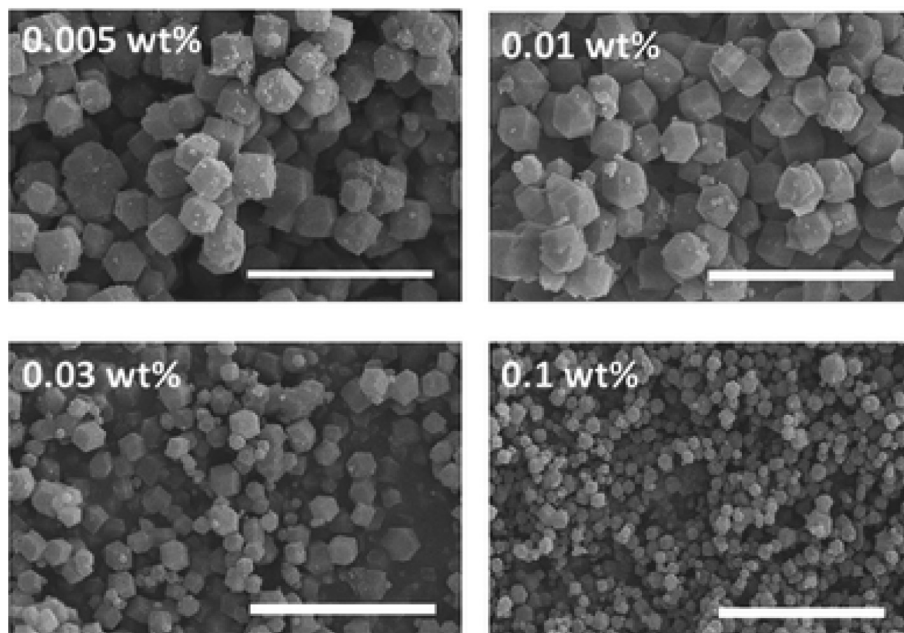


Fig. 5. Scanning electron micrographs (SEM) images of ZIF-8 containing various amounts of gelatin (0.005–0.1 wt%). The scale bar is 10 nm. Reproduced with permission [50]. Copyright 2013 The Royal Society of Chemistry.

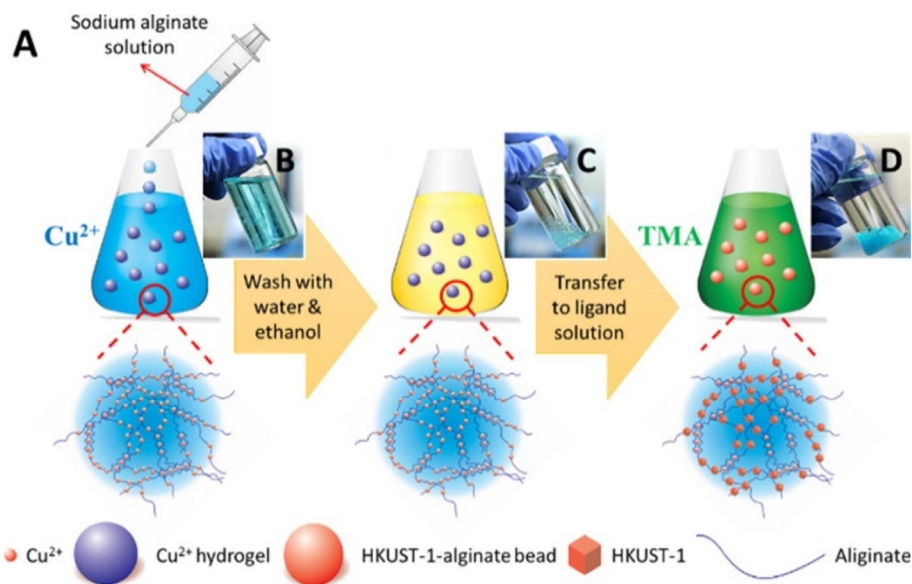


Fig. 6. (a) The preparation of the MOFs-alginate hydrogel composite. (b) Alginate hydrogels cross-linked by Cu^{2+} ions after adding a sodium alginate aqueous solution to a Cu^{2+} aqueous solution. (c) Alginate hydrogels cross-linked by Cu^{2+} ions after being washed with water and ethanol. (d) The photograph of HKUST-1-alginate hydrogels. Reproduced with permission [53]. Copyright 2016 American Chemical Society.

3.1.1. Pure MOF hydrogels

Yin et al. reported lanthanide MOF hydrogels with intrinsic and tunable emission color [49]. These hydrogels were prepared with 5-boronisophthalic acid and Tb^{3+} , Eu^{3+} , or Dy^{3+} ions similar to the common MOFs. The gels exhibited intrinsic trichromatic fluorescence, because the full-color emissions can be obtained by tuning the type or ratio of lanthanide ions. The lanthanide ions and 5-boronisophthalic acid formed separate layers. Then, these layers grow anisotropically to form nanoribbons, which are further wound together to produce hydrogels. Yin et al. poured Eu-Tb-Dy MOF hydrogels with various Eu/Dy/Tb ratios into separate molds to explore their ability. As shown in Fig. 4, Eu-Tb-Dy MOF hydrogels can be shaped into different shapes, indicating their tunable

shape. All the hydrogels possess the same color under sunlight, however, under single-wavelength excitation at 275 nm, their color difference is very obvious. This work provides a new method of the design of flexible and soft MOFs hydrogels for extensive applications in the future.

3.1.2. MOF@biology derived organic macromolecules hydrogels

Biology-derived organic macromolecules are undoubtedly ideal materials, because they come from nature. Biology-derived organic macromolecules are able to combine low costs, sustainable production, and environmental protection. The usage of biology-derived organic macromolecules as matrixes for MOF growth is rarely explored.

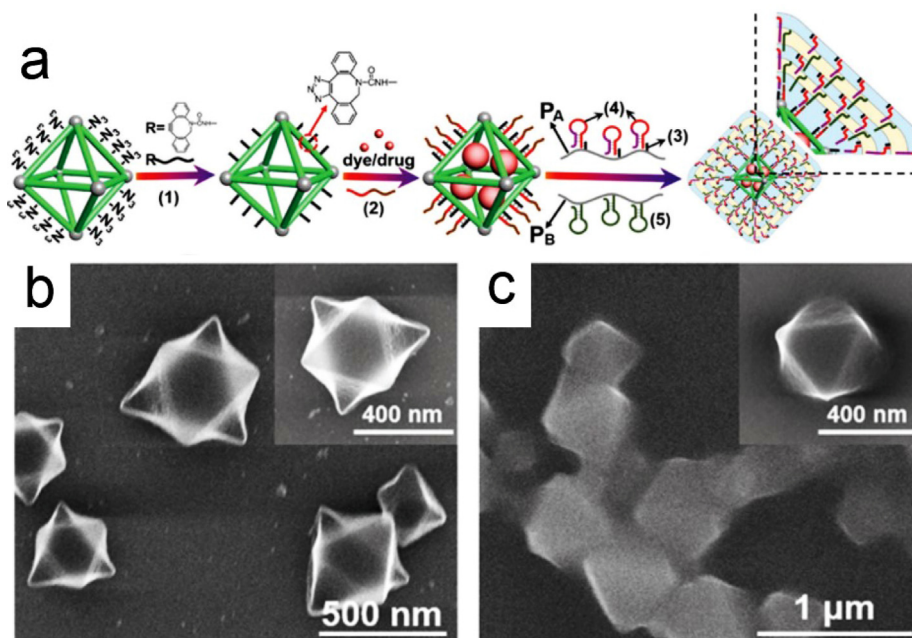


Fig. 7. (a) Synthesis of DNA/polyacrylamide-hydrogel-coated MOFs loaded with dye or drug. (b) Typical SEM image of the MOFs. (c) Typical SEM image of the MOFs coated with hydrogel. Reproduced with permission [56]. Copyright 2017 Wiley-VCH Verlag GmbH & Co. KGaA, Weinheim.

Gelatin is a protein partially hydrolyzed by the collagen of bones, skins, hoofs and tendons of cows, pigs, fish, or other animals [65]. Bradshaw and coworkers employed a biomineral-inspired method to grow two classical MOFs (ZIF-8 and HKUST-1) in a cheap non-toxic gelatin hydrogel as a matrix [50]. The approach was to add metal salts during the gelatin formation process to form cation-embedded hydrogels. Through the addition of metal salt solutions containing 1-hexyl-3-methylimidazolium or trimesic acid, ZIF-8 or HKUST-1 crystals can be obtained respectively. In addition, gelatin hydrogel can be used as a modifier of macromolecular crystal growth to change the crystal growth degree of two MOFs, which is similar to natural biomineralization. As shown in Fig. 5, the amount of the added gelatin can greatly change the crystalline size of the ZIF-8 inside the matrix to meet different application requirements.

Chitosan is derived from chitin, which is widespread found in the shell of crustaceans, the shell of insects and the cell wall of fungi. Wang et al. prepared ZIF-8/chitosan composites in the chitosan hydrogel matrix [66], where chitosan was interpenetrated with ZIF-8 crystals. The existence of chitosan greatly changed the size of ZIF-8 crystals, because the oxhydryl and amino groups of chitosan would affect the exposure of the crystal surfaces. Cui

and coworkers embedded carbonic anhydrase molecules into ZIF-8 (CA@ZIF-8) [51]. Then, this composite was encapsulated in the poly(vinylalcohol)-chitosan hydrogel to prepare composite hydrogel. The immobilization efficiency of carbonic anhydrase molecules was more than 70%, indicating its high immobilization efficiency. Compared with carbonic anhydrase and CA@ZIF-8 composite, the as-prepared composite hydrogel displayed better mechanical strength, stability, and reusability.

Agarose is a type of polysaccharide extracted from the plant (Rhodophyceae). Because of its special gelling properties, agarose has been widely used in many fields. The composite between MOFs and Agarose can also be synthesized by using agarose hydrogel as the matrix. Huang and coworkers incorporated a fluorescent dye (Rhodamine B (RhB)) into stable UiO-66-NH₂ (a Zr-based MOF) [52]. Then, this material was dissolved in hot ultrapure water with dispersed agarose powder. The solution was transferred into a 96-well plate and cooled down to obtain MOF-based agarose hydrogel. Owing to its portable, robust, and convenient-synthesis characteristics, this MOF-based agarose hydrogel was expected to show potential in field of clinical diagnosis. In addition, this synthetic method is expected to be able to prepare more composites between stable MOFs and agarose hydrogel.

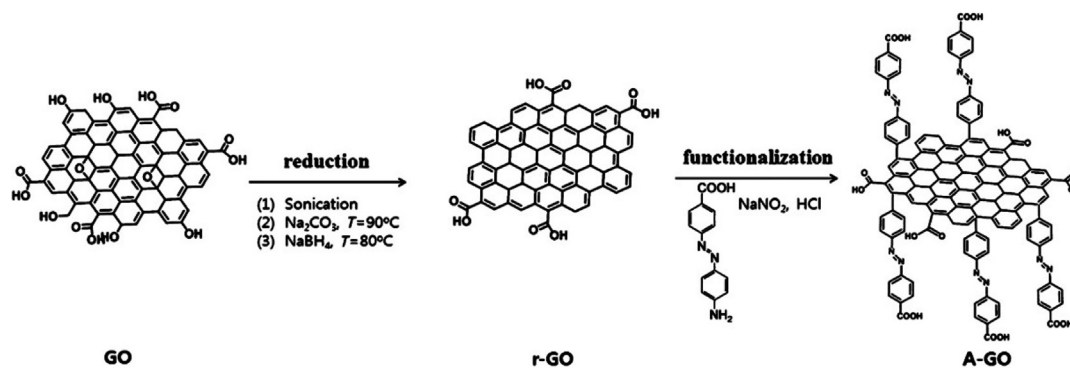


Fig. 8. The typical method to synthesize A-GO. Reproduced with permission [58]. Copyright 2011 Wiley-VCH Verlag GmbH & Co. KGaA, Weinheim.

Later on, a series of alginate hydrogels have been fabricated. As shown in Fig. 6, the cation cross-linked hydrogels are a good candidate to prepare MOFs-based composites for lithium adsorption, water purification, and the diagnosis of penicillin allergy [53]. Especially, Zhao et al. prepared a hydrogel microfiber containing vitamin MOFs through microfluidic spinning method [54]. The alginate hydrogel shell was formed by the rapid gelation reaction between sodium alginate and calcium chloride from the two-phase solution in the microfluidic system. At the same time, nicotinic acid (vitamin B3) solution and copper acetate or zinc acetate solution were injected into the fiber sheath as the precursors of MOFs, and then, copper-vitamin or zinc-vitamin MOF were formed *in situ* in the hollow hydrogel shell.

3.1.3. MOF@biocompatible hydrogels

Biocompatible hydrogels play an important role in several fields such as drug delivery and wound healing, however, they are often limited by their instability [67]. To address this issue, the addition of MOFs in biocompatible hydrogels might be a good strategy to improve the mechanical properties of biocompatible hydrogels. Harmon and coworkers designed a zeolite-like MOF to enhance the property of N-vinyl-2-pyrrolidinone hydrogel [55]. The as-obtained composites had a net covering the pores and exhibited the better mechanical stability in water than that of N-vinyl-2-pyrrolidinone hydrogel without zeolite-like MOF.

Willner et al. employed MOF nanoparticles to support anticancer drug doxorubicin and coated a stimulatory-responsive polyacrylamide/DNA hydrogel [56]. The cross-linking of this hydrogel was carried out in cage structure by nucleic acid double chains containing anti-adenosine triphosphate aptamers. Fig. 7 shows the schematic diagram and morphology of hydrogel-coated MOF nanoparticles. As shown in Fig. 7a, after synthesizing MOF material (UiO-68), the amino functional groups on its surface were converted into azide functional groups to link the modified nucleic acid. The anticancer drug doxorubicin was then loaded into the UiO-68 nanoparticles and the carrier was hybridized to form a double-stranded immobilization unit. Finally, these nanoparticles were further precipitated and suspended in buffer solution

containing DNA functional acrylamide chains with two hairpins. As shown in Fig. 7b and 7c, the UiO-68 nanoparticles exhibit a double pyramid structure with a size between 280 and 350 nm. After hydrogel coating, the sharp angle of the UiO-68 nanoparticles disappears, and the surface of the particles becomes smooth.

Copper ion shows bright prospects in the healing of chronic non-healing wounds. Excessive use of copper salts or copper oxides, however, may cause the wound to deteriorate. To solve this problem, Ameer et al. embedded copper MOF nanoparticles (named as HKUST-1 NPs) within an antioxidant thermo-responsive citrate-based hydrogel (poly-(polyethyleneglycol citrate-co-N-isopropylacrylamide), named as PPCN) [57]. This method can accelerate wound healing and decrease the toxicity of copper ions. This report further confirms that biologically-incompatible MOF materials wrapped in biocompatible hydrogels can play a specific role in the field of biomedicine.

3.1.4. MOF@graphene hydrogels

As a new kind of carbon materials, the study of graphene materials, including graphene, graphene oxide (GO), and reduced graphene oxide (rGO), is very hot in the fields of chemical science and material science [68]. Graphene materials are well characterized by their 3D graphene network, excellent conductivity, and rich functional group structures [69].

As shown in Fig. 8, Jung et al. efficiently synthesized a derivative of GO by using a two-step reaction method [58]. The derivative was named as A-GO. The A-GO can produce a MOF-GO composite hydrogel (named as MOF-A-GO) by mixing with organic ligands (Fig. 9a) in the presence of Zn^{2+} ions. Fig. 9b shows the appearance and fluorescence characteristic of the resulting hydrogel. As shown in Fig. 9c, the morphology of MOF-A-GO is quite different from that of common GO nanosheets. MOF-A-GO has a nanorod structure with a length of several micrometers and a width of 100–150 nm. It indicates that A-GO and organic ligands are well bonded and arranged in an order manner to form a well-arranged structure.

Yan and coworkers used modified Hummer's method to prepare GO powder, which can be dispersed in water [59]. Ascorbic acid

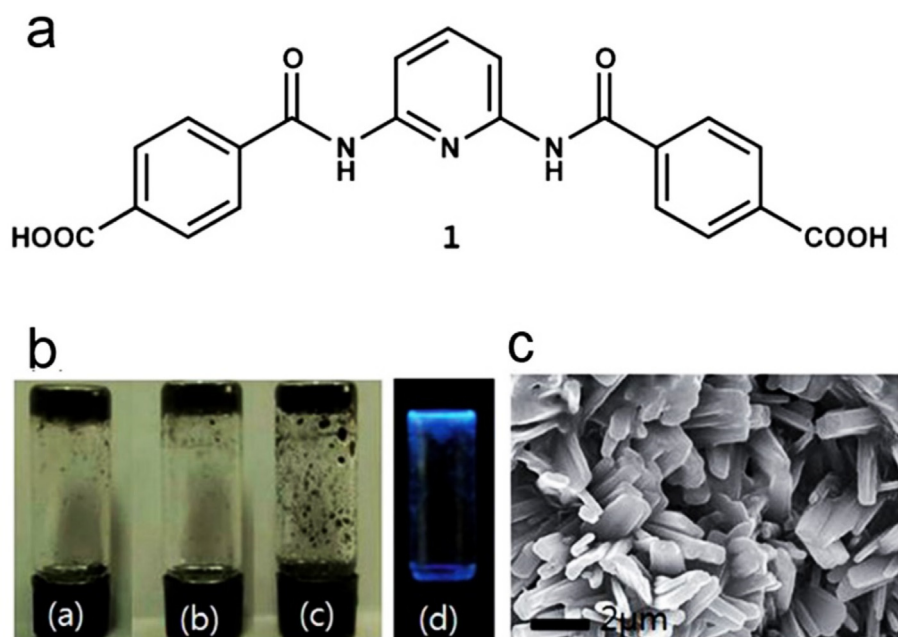


Fig. 9. (a) The typical formula of ligand 1. (b) The Photographs of MOF-A-GO composite hydrogels. (c) The typical SEM image of a MOF-A-GO composite hydrogel. Reproduced with permission [58]. Copyright 2011 Wiley-VCH Verlag GmbH & Co. KGaA, Weinheim.

and sodium hydrate were added into the GO solution. Then, the mixed solution was heated to gain the graphene hydrogel, which was further immersed in methyl alcohol containing zinc nitrate hexahydrate and 2-methylimidazole. After a period of reaction, ZIF-8 would grow in the network of graphene hydrogel. The obtained ZIF-8/graphene hydrogel nanocomposite is stable in alkaline solution.

In addition to the MOF-based hydrogels mentioned above, there are other types of MOF-based hydrogels such as ZIF-8/laponite clay hydrogel nanocomposite and HKUST-1@PVA-co-PE/PVA hybrid hydrogel [60,61]. Overall, there are not many types of MOF-based hydrogels. Besides, with the attention paid to environmental protection, recycling and other related fields, the demand for stimulus response and self-repairing hydrogels is increasing day by day. Thus, more exploration in this direction is highly desirable.

3.2. MOF-based aerogels

Aerogels are multifunctional materials with 3D interconnected gel networks, and often prepared by sol-gel approach and supercritical drying processing [70,71]. A variety of aerogels such as silica aerogels, metal oxide aerogels, polymeric aerogels, carbon-based aerogels, semiconductor chalcogenide aerogels and protein-based aerogels have been studied [45]. By using aerogels as the matrixes, MOF crystals can be inserted into them and become more stable. We summarized MOF-based aerogels in Table 2. Apart from pure MOF aerogels, MOF-derived aerogels can be categorized into four primary types in terms of their material compositions: MOF@silica aerogel composites, MOF@graphene aerogel composites, MOF@cellulose aerogel composites, and aerogel composites containing MOFs-derived materials. Besides, there are some special aerogels with especial complex composition.

Table 2
The summary of MOF-based aerogels.

MOF	Matrix	Application	Ref
MIL-100 (Fe)	–	–	[72]
Cr-BTC	–	Dye adsorption	[73]
Al (III)-carboxylate	–	absorbent	[74]
UiO-66	–	–	[75]
UiO-67	–	–	[75]
UiO-66-NH ₂	–	–	[75]
HKUST-1	silica aerogel	–	[76]
HKUST-1	silica aerogel	Chromatographic material	[77]
HKUST-1	silica aerogel	–	[78]
ZIF-8	silica aerogel	–	[79]
MIL-101	graphene oxide aerogel	Drug extraction	[80]
ZIF-8	graphene aerogel	CO ₂ adsorption	[81]
ZIF-8	graphene aerogel	Particulate Matter Capturing	[82]
MIL-88-Fe	graphene aerogel	Supercapacitors	[83]
HKUST-1	Ru/graphene aerogel	Catalytic CO Oxidation	[84]
ZIF-8	reduced graphene oxide aerogel	water remediation	[85]
polypyrrole@ZIF-8	graphene aerogel	sensing	[86]
ZIF-8	cellulose nanocrystal	–	[87]
UiO-66	cellulose nanocrystal	–	[87]
MIL-100 (Fe)	cellulose nanocrystal	–	[87]
ZIF-8	cellulose nanocrystal-carboxymethyl cellulose	–	[87]
UiO-66	cellulose nanocrystal-carboxymethyl cellulose	–	[87]
MIL-100 (Fe)	cellulose nanocrystal-carboxymethyl cellulose	–	[87]
ZIF-9	cellulose aerogel	Water treatment	[88]
ZIF-12	cellulose aerogel	Water treatment	[88]
ZIF-67-derived Co/C composites	polypyrrole hydrogel	Electromagnetic absorption	[89]
Prussian blue-derived Fe ₂ O ₃	graphene aerogel	Lithium-Ion Battery	[90]
MOF (Fe)-derived Fe ₂ O ₃	reduced graphene oxide aerogel	Supercapacitor	[91]
MOF (Ni)-derived NiO/Ni	reduced graphene oxide aerogel	Supercapacitor	[91]
MOF (Fe)-derived Fe ₂ O ₃	nitrogen-doped graphene aerogel	Oxygen reduction reaction	[92]
MOF (Co)-derived CoO _x	nitrogen-doped graphene aerogel	Oxygen reduction reaction	[93]
MOF (Co)-derived Co nanoparticles	nitrogen-doped graphene aerogel	Hydrogen evolution reaction and oxygen reduction reaction	[94]
ZIF-67 derived Co ₃ O ₄	carbon aerogel	Supercapacitor	[95]
ZIF-8/C ₃ N ₄	agar aerogel	Water treatment	[96]
Cu-BTC	Titania aerogel	photon absorption	[97]
[Zn(N-(4-pyridylmethyl)-l-valine-HCl)(Cl)](H ₂ O) ₂	Titania aerogel	dye-sensitized solar cell	[98]
ZIF-8	Konjac glucomannan	Water treatment	[99]
Ni/Co-MOF	CMC aerogel	Water treatment	[100]
Tb (III)-based metal-organic gel	–	Sensing	[101]
Eu (III)-based metal-organic gel	–	Sensing	[102]
HKUST-1@Fe ₃ O ₄ particles	–	–	[103]
ZIF-8	PolyHIPEs	–	[104]
UiO-66	PolyHIPEs	–	[104]
Cr-MIL-101	PolyHIPEs	–	[104]
HKUST-1	PolyHIPEs	–	[104]
HKUST-1	MMPam	catalysis	[105]
MOF-2	MMPam	–	[105]
UiO-66	MMPam	–	[105]
Fe-MIL-101(-NH ₂)	MMPam	–	[105]

3.2.1. Pure MOF aerogels

MIL-100 constructed from iron ions and benzene tricarboxylates have been reported as a typical MOF. Besides, MIL-100 is also the first MOF aerogel synthesized in a sol-gel approach, followed by supercritical carbon dioxide (CO₂) drying in a particular reaction container. Kaskel and co-workers have reported that MIL-100 aerogel possessed a structure of lower density as compared to the air-dried powdered MIL-100 sample, and showed a higher degree of macroporosity (Fig. 10). The specific surface areas and micropore (diameter < 2 nm) volumes were given 1183 m² g⁻¹, 0.52 cm³ g⁻¹ and 1618 m² g⁻¹, 0.72 cm³ g⁻¹ for the powdered MIL-100 and MIL-100 aerogel, respectively. The coexistence of microporosity and macroporosity is decisive for the catalysis or storage applications of MIL-100 aerogel without mass transport restrictions [72]. Notably, this work pioneered the technique to prepare monolithic MOF aerogels with various shapes and sizes through changing the reaction containers, which opened novel possibilities in the industrial application of MOFs.

Zhang et al. designed a new method to produce a range of Cr (III) porous aerogels and Fe (III) porous aerogels with different rigid bridging carboxylic ligands, including BTC, BDC, ADC, NDC, FDC, BuDC, and BTB. These aerogels with large void spaces were

synthesized in a sol-gel approach at 80 °C, followed by solvent exchange and supercritical CO₂ drying. By using rigid carboxylate ligands such as 1,4-BDC and 1,3,5-BTC, various MOFs could be prepared, then leading to highly porous aerogels. These aerogels had high surface areas and satisfied porous structures with microporosity and mesoporosity. It is worth pointing out that the porosity of Cr-BTC aerogel could be tuned by changing the reactant concentrations. The Cr-BTC aerogel is mainly microporous at high reactant concentrations, while the hierarchical porous aerogel with mesopore (2 nm < diameter < 50 nm) can be obtained at lower reactant concentrations [73]. This work represented a strategy to prepare organic-inorganic hybrid aerogels with various frameworks for adsorption. Moreover, porous Al (III)-carboxylate aerogels could be produced by the mismatched growth-gelation of MOF nanoparticles, followed by CO₂ extraction [74].

In order to directly utilize Zr⁴⁺ based MOF aerogels for adsorptive and catalytic applications, three kinds of Zr⁴⁺-based MOF aerogel monoliths (including UiO-66, UiO-67, and UiO-66-NH₂) were presented. After sol-gel approach, the as-resulted gels can be dried under supercritical CO₂ to reap Zr⁴⁺ based MOF aerogels. Especially, monolithic UiO-66 spheres with uniform and adjustable diameter were prepared by using an oil-drop method. Unlike pow-

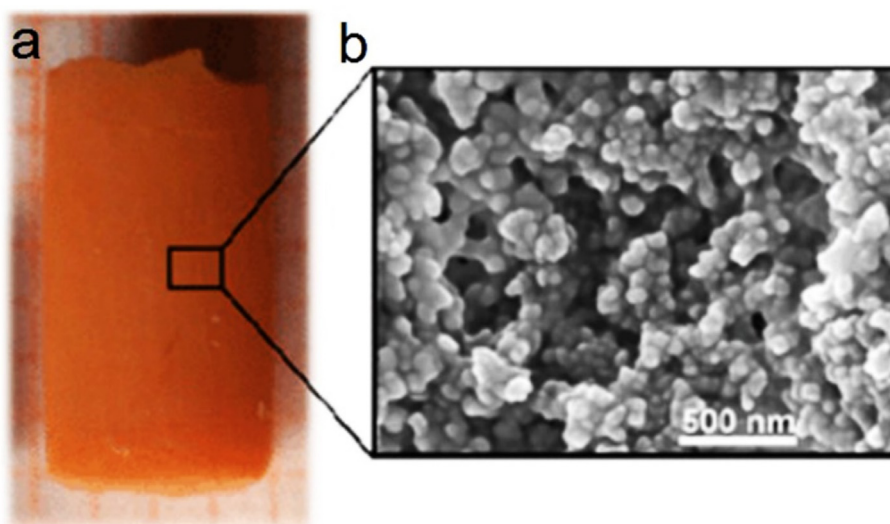


Fig. 10. (a) The photograph of the MIL-100 aerogel. (b) The typical SEM image of the MIL-100 aerogel. Reproduced with permission [72]. Copyright 2009 The Royal Society of Chemistry.

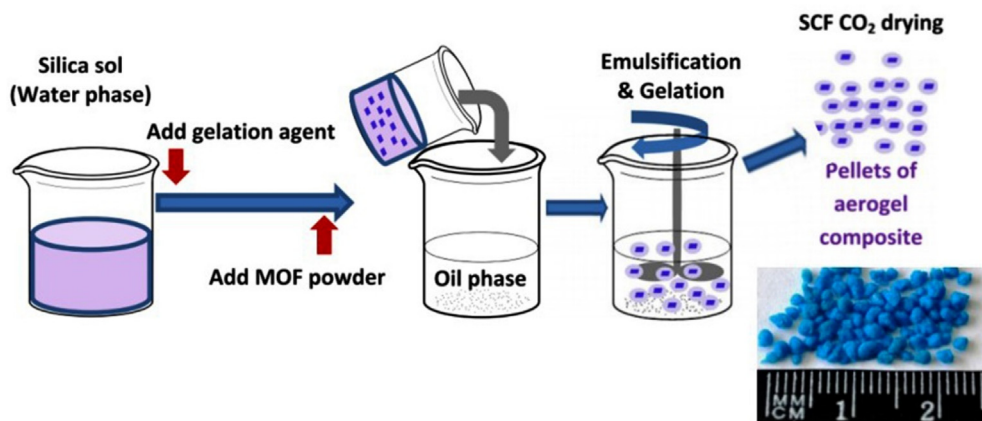


Fig. 11. The synthesis process of HKUST-1@silica aerogel pellets and their photograph. Reproduced with permission [78]. Copyright 2017 Springer Science Business Media, LLC.

dered UiO-66 bulk, UiO-66 spheres possessed large pore volumes and hierarchical pore system, which can facilitate mass transfer. Moreover, this is a convenient way to prepare MOF aerogels with a hierarchical structure, which can be directly used for industrial adsorptive applications or packed-bed catalytic [75].

3.2.2. MOF@silica aerogel composites

There are many methods for synthesizing MOF-silica composites to improve their mechanical properties [106,107]. Among different types of nanoporous silica materials, silica aerogels are considered as appropriate candidates for the varieties of applications because of their attractive properties such as high surface area, narrow pore size distribution, flexible processability, low density, as well as thermal conductivity [45]. Silica aerogels belong to mesoporous materials, which can be synthesized via sol-gel technique. Recently, many researchers have begun to attach the importance onto the study of developing shaped composites of silica aerogels with various guest materials. Besides, designing appropriate approaches of MOFs shaping is a hot topic in the research world. Based on combining silica aerogels with the desirable MOFs, it is possible to produce new shaped MOF@silica aerogel composites for specific applications.

HKUST-1, also known as Cu-BTC, which consists of copper oxide clusters linked by benzene-1, 3, 5-tricarboxylate ligands, is a common MOF material. Erkey et al. synthesized HKUST-1@silica aerogel composites with monolithic structures at the first time by using sol-gel process including hydrolysis, condensation, gelation, curing, solvent exchange, and then supercritical drying. The blue monolithic materials consisted of dispersed microporous HKUST-1 in the silica aerogel with mesoporosity and could be produced in any shape. The microporosity of HKUST-1@silica aerogel composites was increased with the increasing amount of HKUST-1, and the total surface area of these monolithic materials could reach $1138 \text{ m}^2 \text{ g}^{-1}$. Thanks to the rich pore structures, HKUST-1@silica aerogel composites had potential for gas adsorption and gas separation [76]. However, some fraction of monolithic aerogel composites was blocked. In order to overcome this defect, an evolutive approach was exploited for the synthesis of HKUST-1@silica aerogel composites utilizing preparative prepared silicon dioxide (SiO_2) sol as a silica precursor. After adding the HKUST-1 and proceeding sol-gel method, the gel was dried in supercritical CO_2 . This synthetic approach minimized the deterioration of the individual structures of HKUST-1 and silica aerogel, and then prevented the micropores of HKUST-1 from being blocked. The advanced

HKUST-1@silica aerogel composites can tune the properties of themselves and have the potential to be used in the field of chromatographic separation as stationary phases [77]. But during the process to prepare the aerogel pellets for stationary phase, the material must be reshaped, and then nearly 40 percent of the HKUST-1@silica aerogel composites will be wasted in the form of a fine powder. Consequently, the direct synthesis of HKUST-1@silica aerogel composites as pellets has been reported by applying the combination of the sol-gel method and emulsion method. The pellet size can be tuned from 0.1 mm to 2.5 mm by changing the speed of stirring, indicating that the pellets of HKUST-1@silica aerogel composites can meet different application requirements (Fig. 11) [78].

In addition to HKUST-1@silica aerogel composites, there is a novel silica aerogel composite with ZIF-8 prepared by using sol-gel method. The pore characteristics of ZIF-8@silica aerogel composite can be tuned by varying the content of ZIF-8. The composites with different ZIF-8 contents (10, 20 wt%) exhibited different specific surface area in the range of $563\text{--}540 \text{ m}^2 \text{ g}^{-1}$. The ZIF-8 crystals in silica aerogels were clearly showed by using transmission electron microscope (TEM). Owing to its pore sizes and structures, the potential application fields of ZIF-8@silica aerogel composites are diverse, such as adsorption, catalysis, and energy devices [79].

It is worth noting that typical silica aerogels are very brittle and fragile under stress, especially at high temperatures or sudden thermal shocks. Conventional strategies for reducing the brittleness of the silica aerogel often result in a reduction in other properties. As a result, many flexible aerogels have been developed.

3.2.3. MOF@graphene aerogel composites

Graphene aerogel (GA) has lower density, higher compressibility, higher specific surface area, and better electrical conductivity than other graphene macrostructures [108]. More importantly, GAs can be used as reliable matrixes for depositing numerous nanomaterials such as MOFs, which could achieve enhanced applied performances due to the synergistic effects. For example, the synergistic effects of GA and MOF can enhance the performance as supercapacitor materials, because the rich pore structure and large specific surface area of MOF can provide a large number of electron adsorption sites and GA can provide strong conductivity.

Ding et al. first reported the importance and application potential of MOF@graphene aerogel composites. They synthesized

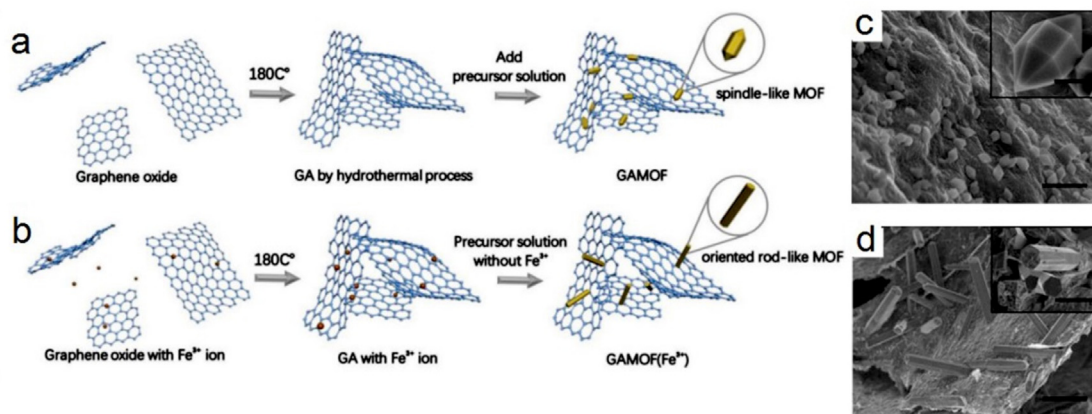


Fig. 12. (a) The schematic illustration of the synthesis process of the spindle-like MOF@GA. (b) The schematic illustration of the synthesis process of rod-like MOF@GA. (c) SEM images of the spindle-like MOF@GA (scale bar: $2 \mu\text{m}$) and the corresponding high-magnification SEM images (inset; scale bar: 500 nm). (d) SEM images of the rod-like MOF@GA (scale bar: $2 \mu\text{m}$) and the corresponding high-magnification SEM images (inset; scale bar: 500 nm). Reproduced with permission [83]. Copyright 2018 Wiley-VCH Verlag GmbH & Co. KGaA, Weinheim.

MIL-101@graphene oxide hybrid aerogels with a 3D architecture by a “sol-cryo” method without using any templates [80]. In order to simplify the preparation process of MIL-101@graphene oxide hybrid aerogel, Xing et al. synthesized MIL-101 by hydrothermal method, and then mixed the as-synthesized MIL-101 with graphene oxide [109]. After hydrothermal and freeze drying, the MIL-101@graphene oxide hybrid aerogel was simply synthesized. After the emergence of MIL-101@graphene oxide hybrid aerogel, more similar aerogels had appeared. ZIF-67@graphene hybrid aerogel was synthesized by using a counter diffusion method. The ZIF nanoparticles of the aerogel uniformly dispersed in the 3D macroporous framework of graphene sheets. Hierarchically porous ZIF-8@graphene hybrid aerogel was prepared by a two-step reduction strategy and a layer-by-layer assembly method. This energy-saving synthesis strategy can avoid tedious dry step and power-wasting freeze-drying technology [81]. Besides, a novel strategy to decorate ZIF-8 crystals on graphene aerogel by combining *in situ* crystallization of ZIF-8 crystals with naturally drying the resultant hydrogel [82]. Interestingly, scientists found that changing the adding time of ligands could alter the morphology of MOF. To synthesize MIL-88-Fe@GA, adding iron ion and 1,4-benzenedicarboxylate (H_2BDC) ligand solutions into GA solution can produce spindle-like MIL-88-Fe (spindle-like MOF@GA). On the contrary, the morphology of MIL-88-Fe is rod-like (rod-like MOF@GA) when the ligand solution was added into previously-treated homogeneous mixed solution of iron ion and GA (Fig. 12) [83]. Obviously, different morphologies of MIL-88-Fe can lead to different physical properties, which make it possible for different applications. In some catalytic applications, noble metals, such as Pt and Ru, are needed to be loaded into graphene aerogel. Some novel aerogels can be synthesized by combining MOF and graphene aerogel loading noble metals (noble metals/GA) because of the macroporous structure of the noble metals/GA. As a typical example, Ru/GA-HKUST-1 with excellent compressibility was synthesized by decorating HKUST-1 on the Ru/GA surface via using solvothermal synthesis and step-by-step self-assembly method. HKUST-1 nanoparticles uniformly dispersed on the surface of GA and maintained the structure well [84]. Besides, in order to obtain MOF@rGO aerogel composites, it is necessary to add reductants after synthesizing GO, such as hydrazine hydrate and vitamin C. As a typical example, ZIF-8@rGO aerogel was synthesized with synergistic effects of chemical reduction and cross-linking by

metal ions. After reduction process, the oxygen-containing groups of GO were removed, and the π - π stacking interactions were enhanced to form relatively ordered pore structures [85]. Furthermore, the MIL-101@GO hybrid aerogel mentioned above can be reduced to MIL-101@rGO hybrid aerogel under the treatment of hydrazine vapor [80]. These methods of the as-obtained MOF@rGO aerogel composites with relatively ordered pore structures can produce many new aerogels based on rGO and MOF, which can be applied in different fields including energy and environment. Recently, scientists have also reported on ternary aerogel composites, such as polypyrrole@ZIF-8/graphene aerogel. It is reasonable to believe that the composition and properties of ternary aerogel composites are expected to be further tuned and enhanced. Apart from such MOF@graphene aerogel composite materials, there is a variety of MOF-derived material@graphene hybrid aerogels mentioned frequently, which are mentioned in the following Section 2.2.5.

All of the above-mentioned MOF@graphene aerogel composites can maintain the characteristics of the aerogels and embed MOFs. However, compared with these aerogels, superelastic hard carbon nanofiber aerogel shows great advantages in mechanical strength and structural stability [110]. Therefore, it is very meaningful to explore its composite aerogel with MOFs.

3.2.4. MOF@cellulose aerogel composites

Cellulose is one of the most abundant renewable polymer materials stored in nature. It can be extracted from cotton, wood, hemp, bamboo and crop straw. Cellulose is considered to be the main raw material in the energy and chemical fields in the future due to its wide source, renewable property, high specific surface area, low cost, complete biodegradation and easy physical or chemical modification [111]. The shape ability and mechanical flexibility of cellulose aerogels rely on their cross-linking, pore structure, intrinsic toughness, and dimensionality [112]. Cellulose has moderate diameter and offers the opportunity of producing a fibrous porous matrix, which can be combined with MOFs to produce novel aerogel composites. This combination approach can effectively address the challenge to improve the processability and handling of MOFs, however, such approach didn't receive much attention until Cranston and coworkers discovered cellulose nanocrystal (CNC)-cross-linkable carboxymethyl cellulose (CMC) based MOF hybrid aerogels (CNC:CMC:MOF = 1:1:1 by weight)

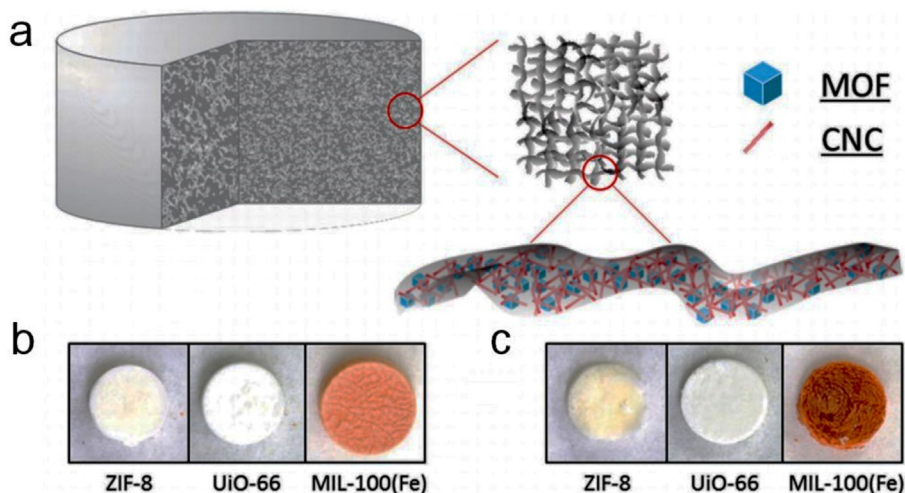


Fig. 13. (a) The schematic of the designed MOF-cellulose hybrid aerogel. (b) The photographs of cellulose nanocrystal (CNC)-carboxymethyl cellulose (CMC) based hybrid aerogels (CNC:CMC:MOF = 1:1:1 by weight). (c) Photographs of all-CNC based hybrid aerogels (CNC:CNC:MOF = 1:1:1 by weight). The diameter of all aerogels is about 7 mm and the height of all aerogels is about 5 mm. Reproduced with permission [87]. Copyright 2016 Wiley-VCH Verlag GmbH & Co. KGaA, Weinheim.

and all-CNC based MOF hybrid aerogels (CNC:CNC:MOF = 1:1:1 by weight) [87]. The MOFs in the hybrid aerogels included ZIF-8, UiO-66, and MIL-100(Fe) (Fig. 13). The hybrid aerogels were prepared by using a sol-gel process, and followed by freeze-drying. The synthesis of these materials was based on orthogonally functionalized celluloses prepared by straight-forward water-based chemistry to impart crosslinking ability. When pre-synthesized MOFs and celluloses were mixed together, celluloses would assemble into cross-linked clusters with pre-synthesized MOFs. After this study, more MOF@cellulose aerogel composites with different structures were synthesized and reported, such as ZIF-9@cellulose aerogel and ZIF-12@cellulose aerogel [88]. Besides, to pursue simplification, the synthetic processes of ZIF-9@cellulose aerogel and ZIF-12@cellulose aerogel were optimized to avoid the pre-synthesis of MOFs. For example, in order to synthesize ZIF-9@cellulose aerogel hybrids, scientists mixed Co^{2+} ions (acting as coordination centers) and cellulose aerogels together, then added benzimidazole solution to form ZIF-9. ZIF-9@cellulose aerogel could be expediently obtained by freeze-drying. The innovative combination of two emerging materials, including celluloses and MOFs, not only contributes to the development of material science, but also shows satisfactory potential in adsorption, separations, and catalysis applications. The preparation of MOF@cellulose aerogel composites with special properties by physical or chemical modification is the development direction in the future. Besides, the development of clean and efficient solvents, as well as low-cost industrial preparation technology, is also necessary.

3.2.5. MOF@organic polymers aerogel composites

In the field of chemical materials, polymers have been paid more and more attention because of their various kinds and functions. So far, some polymers have also been used as the matrixes to synthesize MOF@organic polymers aerogel composites. Generally, magnetic nanoparticles combined with MOFs can produce magnetic composites. However, the pores of MOFs part will be blocked and result in some adverse effects. Bradshaw and coworkers used a pre-synthesized magnetic macroporous polymer as the aerogel matrix for growth of MOFs, as shown in Fig. 14 [105]. The polymer was magnetic macroporous polyacrylamides (MMPam), and the obtained aerogel composite was named as MOF@MMPam. Many MOFs can participate these aerogel composites, including

HKUST-1, MOF-2, UiO-66, and Fe-MIL-101($-\text{NH}_2$). The final aerogel products had excellent magnetic properties, and the structures of MOFs in the pores of aerogels can be well retained.

Besides, they reported another similar strategy. Some MOF particles, including ZIF-8, UiO-66, Cr-MIL-101, and HKUST-1 have been incorporated into the PolyHIPEs composites [104]. PolyHIPEs are porous polymers derived from high internal phase emulsions (HIPEs). The size of pores within the HIPEs can be controlled via changing the amount of MOF crystals, and the final composites can be shaped into any shape. The as-obtained porous MOF/PolyHIPEs composites exhibited robust mechanical properties. In addition, no shape change or deformation was observed under pressure, indicating their bright application prospect.

MOF crystals are always insoluble in solvents and not thermoplastic, indicating that traditional solvent-based or melting-based techniques are not applicable for MOF crystals. Wang et al. incorporated HKUST-1@ Fe_3O_4 particles and CMC solution to form magnetic fluid and presented a strategy to transform the fluid phase to hydrogel and the subsequent aerogel [103]. This strategy solved the above-mentioned defect that MOF crystals were insoluble. The as-obtained aerogel possessed good recoverability and processability.

3.2.6. Aerogel composites containing MOFs-derived materials

In recent years, MOFs have been used as sacrificial templates benefiting from their structural and compositional features for the synthesis of numerous functional nanomaterials, such as metal-carbon, sulfides, oxides, etc. Generally speaking, preparing MOF-derived materials depends on a thermolysis process under a certain gaseous atmosphere, including argon, nitrogen, or air, at a high temperature [113]. Based on this synthetic technology as well as the combination of the current research focus of aerogels, some composites of MOFs-derived materials and aerogels, referred to as MOFs-derived materials@aerogel composites in which the aerogels serve as the matrixes for the dispersed growth of MOFs-derived materials, have been successfully synthesized. Polypyrrole (PPy) aerogel decorated with MOF-derived Co/C (Co/C@PPy aerogel composites) was prepared by a self-assembled polymerization method. Co/C composites were prepared by the calcination of ZIF-67 precursors under argon atmosphere. After this step, Co/C composites and pyrrole monomers were mixed together to form polypyrrole

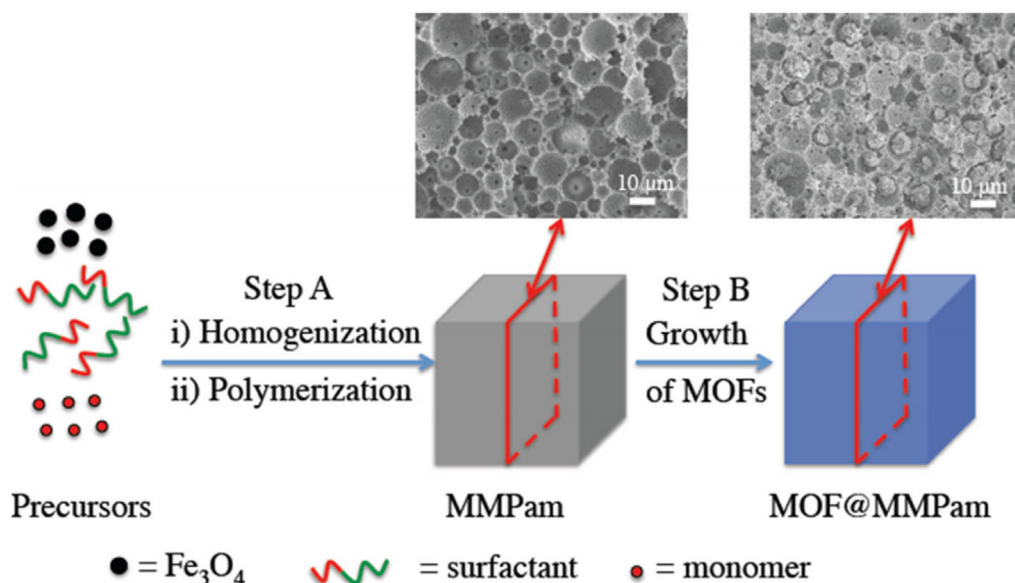


Fig. 14. The synthetic route for the synthesis of MOF@MMPam. Reproduced with permission [105]. Copyright 2019 Springer Science Business Media, LLC.

hydrogel by adding the oxygenant, and then dried at 50 °C to form Co/C@PPy aerogel composites [89]. Similarly, Wang et al. synthesized ZIF-67 derived Co_3O_4 /carbon aerogel [95]. Apart from these exceptional aerogels, all current MOFs-derived materials@aerogel composites are based on graphene aerogel matrixes. Preparation of MOF@graphene aerogel composites followed by specific calcination process is a verified way to obtain MOFs-derived materials@graphene aerogel composites. MOF-derived metal oxides with diversified compositions, porosity, and morphologies are particularly interesting for various applications, because metal oxides possess a variety of functionalities. The method of using MOFs as templates provides an interesting way to prepare metal oxides, such as MoO_3 , ZrO_2 , and Al_2O_3 . For example, based on graphene aerogel matrix and Prussian Blue, Fe_2O_3 @graphene aerogel composite was designed by an excessive metal-ion-induced combination and Ostwald ripening strategy. After calcination process, Prussian Blue could be converted into Fe_2O_3 nanoparticles, which are encapsulated within graphene aerogel [90]. In a similar way, Fe_2O_3 @rGO aerogel composite and NiO/Ni@rGO aerogel composite were produced through freezing-dried and calcination method (Fig. 15) [91]. In addition, in order to obtain nitrogen-doped graphene aerogel, ammonia can be added before the hydrothermal reaction of graphite oxide to synthesize graphene aerogel. To date, these materials mainly include Fe_3O_4 @nitrogen-doped graphene aerogel (NGA) composites and CoOx @NGA composites [92,93]. Particularly, Cui et al reported cobalt-embedded-in nitrogen-doped graphene aerogel composite (Co@NGA) without metal oxides as a superior catalyst. The composite with hierarchical porosity was

synthesized from a MOFs@GA composite through *in situ* hydrothermal assembly method and pyrolysis approach. Co^{2+} was chosen to serve as the central ion which can coordinate with the ligand of 5-Amino-1H-tetrazol to form MOFs [94]. There is no doubt that the above-mentioned aerogel composites containing MOFs-derived materials can expand the range of aerogels and MOFs. Thus, the research and development of these materials should be taken seriously.

3.2.7. Other aerogel composites

In addition to the above-mentioned MOF-based aerogels, there are other types of aerogels. Here, we will list some special and unique MOF-based aerogel composites.

Dispersed ZIF-8 nanoparticles agglomerated on C_3N_4 nanosheets (ZIF-8/ C_3N_4) were integrated into agar aerogel to form an aerogel composite (Fig. 16). Compared with conventional ZIF-8 nanoparticles, ZIF-8 nanoparticles involved in C_3N_4 nanosheets showed smaller size and better dispersity, indicating that C_3N_4 nanosheets can restrict the excessive self-agglomeration of ZIF-8. The crystallinity of the ZIF-8/ C_3N_4 contained in aerogel composite is retained, so the structure and composition of ZIF-8/ C_3N_4 were maintained well after the formation of the agar aerogel composite. The ZIF-8/ C_3N_4 component was encapsulated or embedded within the agar aerogel, thus, the loss of ZIF-8/ C_3N_4 can be minimized during practical application process [96].

Titania (TiO_2) aerogels are of great interest because of their good chemical stability, wide band gap, continuous network, and high specific surface area. Composites containing titania aerogel

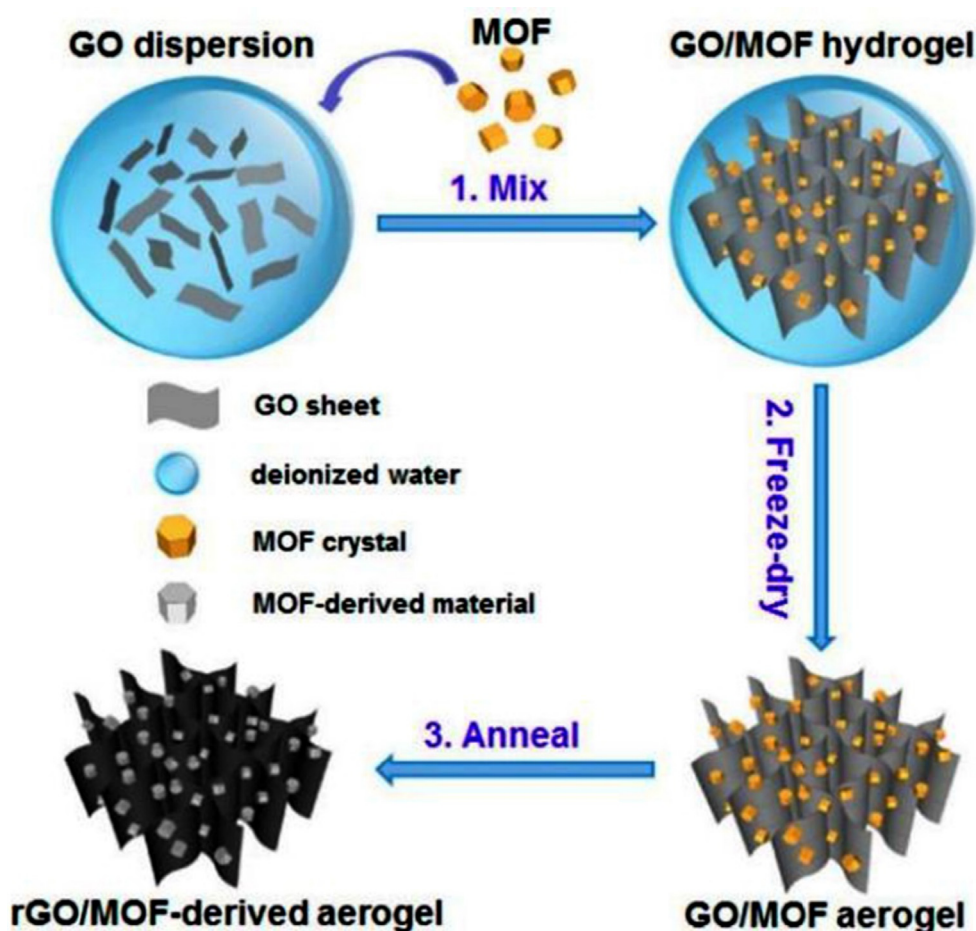


Fig. 15. The typical preparation processes of MOF-derived material@rGO aerogel. Reproduced with permission [91]. Copyright 2017 American Chemical Society.

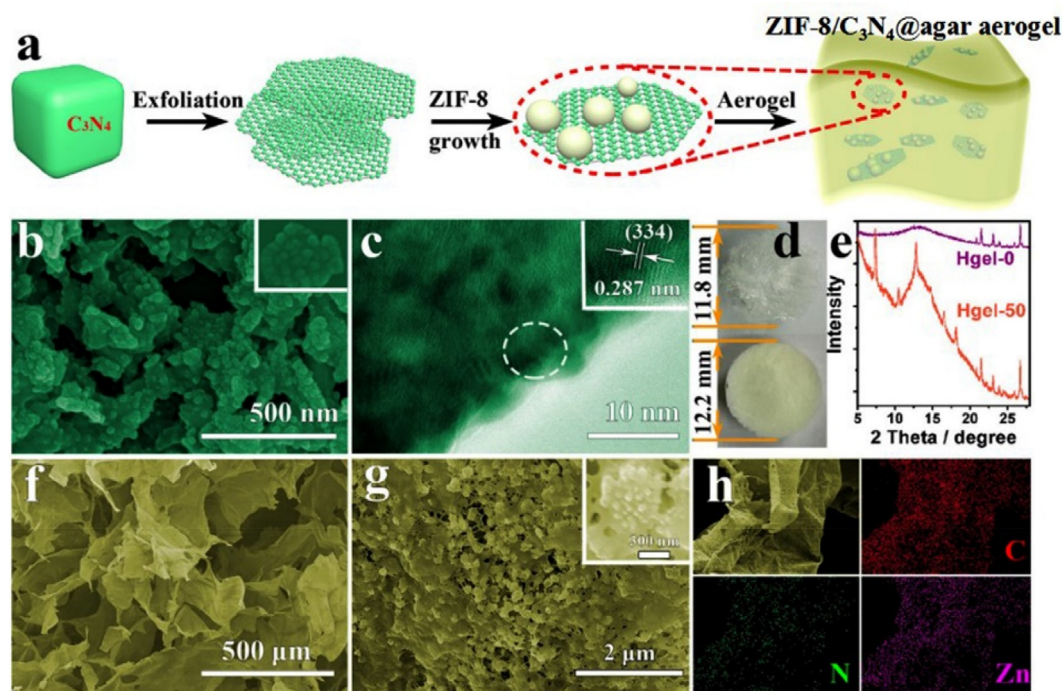


Fig. 16. (a) Schematic illustration of the synthesis of ZIF-8/C₃N₄ heterostructure containing hybrid aerogels. (b) The typical SEM image of ZIF-8/C₃N₄. (c) The HRTEM image of ZIF-8/C₃N₄. (d) Photographs of agar aerogel loading with 0% (top, named as Hgel-0) and 50% (bottom, named as Hgel-50) ZIF-8/C₃N₄. (e) XRD patterns of Hgel-50 and Hgel-0. (f, g) SEM images of agar Hgel-50 at different magnifications. (h) The SEM-EDX elemental mappings of C, N, and Zn elements for ZIF-8/C₃N₄@agar aerogel. Reproduced with permission [96]. Copyright 2017 American Chemical Society.

and MOFs such as Cu-BTC and [Zn(N-(4-pyridylmethyl)-L-valine-HCl)(Cl)](H₂O)₂, were synthesized using sol-gel route followed by subcritical drying technique [97,98]. The aerogel composites are composed of interconnected nanoporous structure which is similar to pristine TiO₂ aerogel. The TiO₂ aerogel acts as the matrix for aerogel composites. MOFs have steadily retained their structural integrity in TiO₂ aerogel matrix and made the aerogel composite more stable.

MOF-based aerogels can be used to fabricate functional devices, however, their industrialized production is inconvenient. Konjac glucomannan (KGM) is abundant in the environment and easily forms aerogels by the deacetylation using sodium carbonate (Na₂CO₃). Besides, 1 mg of KGM can adsorb 0.1 g of water, indicating its low density and good adsorption capacity. Therefore, KGM aerogel is an ideal matrix to immobilize MOFs nanoparticles by forming 3D porous structures in nature. Yan and coworkers prepared plastic KGM-based aerogels combined with ZIF-8 (ZIF-8@KMG aerogel) to enhance the adsorption capacity of KGM. ZIF-8@KMG aerogel was synthesized by using a combination of sol-gel method and freeze-drying process. KGM powder was added to the mixture of ZIF-8 and Na₂CO₃ while stirring. Then, the mixture was covered with a preservative film and placed in a 90 °C environment to form hydrogel. The hydrogel was cooled and freeze-dried to form ZIF-8@KMG aerogel. The ZIF-8@KMG aerogel possessed a smooth surface and uniform pore distribution. Besides, ZIF-8 was dispersedly distributed on the KGM aerogel matrix [99]. This valuable research on KGM-based aerogel has the advantages of portability, flexibility, strong adsorption, green without pollution, easy synthesis, and low cost of raw materials, indicating that KGM aerogel is a promising novel aerogel matrix for MOFs.

However, all of the MOF-based aerogels described above require the pre-synthesis of aerogels. In order to simplify the synthesis process and facilitate large-scale production, using ready-made aerogel templates, such as foams, sponges, and 3D graphene network, is the most convenient method to get the MOF-based

aerogels. These templates possess very stable porous structures and have made promising advances in industrialization. By immersing the template into the mixed solution of ligands and central ions, scientists have made the MOF materials disperse in the pore of the template during solvothermal growth process to produce MOF@template composites. The composites, such as UiO-66@polyurethane foam, MOF-derived ZnCo₂O₄-ZnO-C@ nickel foam, ZIF-8@melamine, MOF-derived octahedral CuO@3D graphene network, and ZIF-8@3D graphene network, maintained the flexibility of the templates, and exhibited the porosity and high surface area of MOFs [114–118]. Combining the inherent advantages of both MOFs and templates, MOF@template composites have more accessibility and higher dispersibility of MOF sites than pristine templates, and better processability, flexibility and portability than powdered MOFs.

4. The applications of MOF-based hydrogels and aerogels

4.1. MOF-based hydrogels

Many matrixes of MOF-based hydrogels come from biological or biocompatible materials, so these hydrogels always have good properties in the biologically-applied fields such as drug release and wound healing. In addition, due to the porous nature of MOFs and hydrogel matrixes, the composite hydrogels of MOFs and hydrogel matrixes have bright prospects in the field of adsorption and sensing.

4.1.1. Drug release

Drug controlled release is a method of using some drug-contained materials to release drugs quantitatively and uniformly in vivo at a constant rate to keep the concentration of drugs in the blood constant [119].

Maji and coworkers synthesized ZIF-8/laponite clay hydrogel nanocomposite, which exhibited a pH-controlled release of encapsulated molecules [60]. In the ZIF-8/laponite clay hydrogel nanocomposite, drug (5-fluorouracil)-encapsulated ZIF-8 nanoparticles were wrapped with laponite layers. The final composite was named as FU@ZIF-8+LP. The release properties of FU@ZIF-8+LP and composites without laponite layers (named as FU@ZIF-8) in acetate buffer (pH 5.0) and phosphate-buffered saline buffer (pH 7.4) differed greatly. The release experiments were monitored over 48 h. In an acetate buffer (pH 5.0), the 5-fluorouracil release rates of FU@ZIF-8 and FU@ZIF-8+LP are high and comparable. More than 90% of 5-fluorouracil was released from both FU@ZIF-8 and FU@ZIF-8+LP within 24 h. This was attributed to the decomposi-

tion of ZIF-8 under acidic conditions. In a phosphate-buffered saline buffer (pH 7.4), FU@ZIF-8 exhibits more than 60% release of the encapsulated 5-fluorouracil within 24 h. As a contrast, less than 15% of 5-fluorouracil is released from the FU@ZIF-8+LP in the first 24 h. It indicates that the undesired loss of 5-fluorouracil could be reduced at physiological conditions (pH 7.4) by using FU@ZIF-8+LP composite.

Polyacrylamide/DNA-hydrogel coated MOFs were utilized to control doxorubicin drug release [56]. Fig. 17a shows the release curves of doxorubicin from polyacrylamide/DNA-hydrogel coated MOFs, indicating the facilitating role of the added ATP. Fig. 17b shows the fluorescence spectra of doxorubicin released from polyacrylamide/DNA-hydrogel coated MOFs at different ATP con-

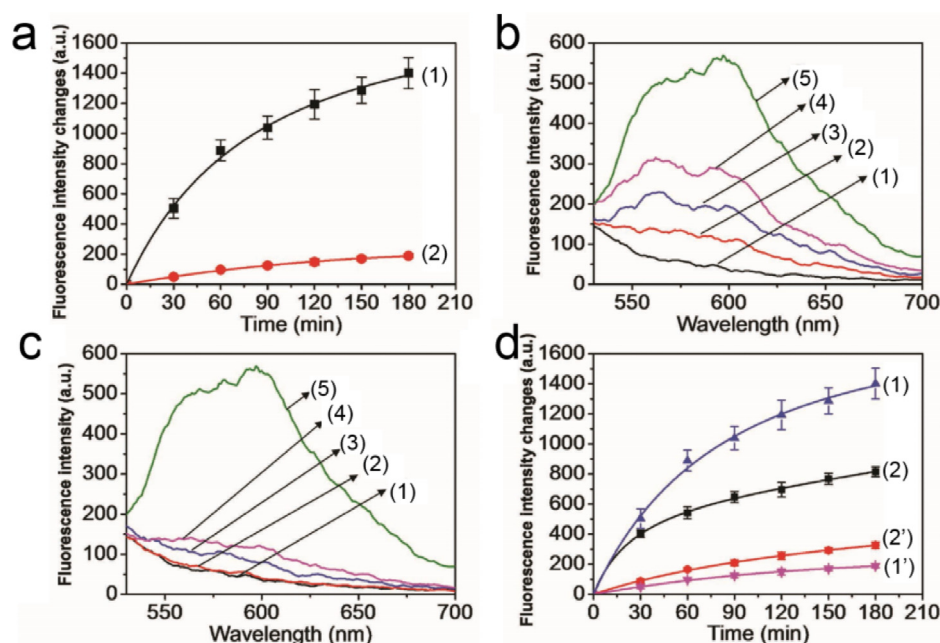


Fig. 17. (a) Curve of release of time-dependent doxorubicin from MOF nanoparticles coated with hydrogel: 1) upon addition of ATP, 50×10^{-3} m, 2) without the addition of ATP. (b) Fluorescence spectra of doxorubicin released from hydrogel coated MOF nanoparticles at different ATP concentrations for a fixed time of 0.5 h: 1) 0×10^{-3} m, 2) 5×10^{-3} m, 3) 10×10^{-3} m, 4) 25×10^{-3} m, 5) 50×10^{-3} m. (c) Selective release of doxorubicin from MOF nanoparticles coated with hydrogel in the presence of: 1) added ATP, 0×10^{-3} m, 2) added TTP, 50×10^{-3} m, 3) added GTP, 50×10^{-3} m, 4) added CTP, 50×10^{-3} m, 5) added ATP, 50×10^{-3} m. (d) Comparison of time-related doxorubicin released/leaked from MOF nanoparticles coated with hydrogel and nucleic acid-terminated MOF nanoparticles: 1) Doxorubicin released from MOF nanoparticles coated with hydrogel under the action of ATP. 2) Doxorubicin released from nucleic acid-terminated MOF nanoparticles under the action of ATP. 1') Doxorubicin leaking from MOF nanoparticles coated with hydrogel without ATP. 2') Doxorubicin released from nucleic acid-terminated MOF nanoparticles without ATP. Reproduced with permission [56]. Copyright 2017 Wiley-VCH Verlag GmbH & Co. KGaA, Weinheim.

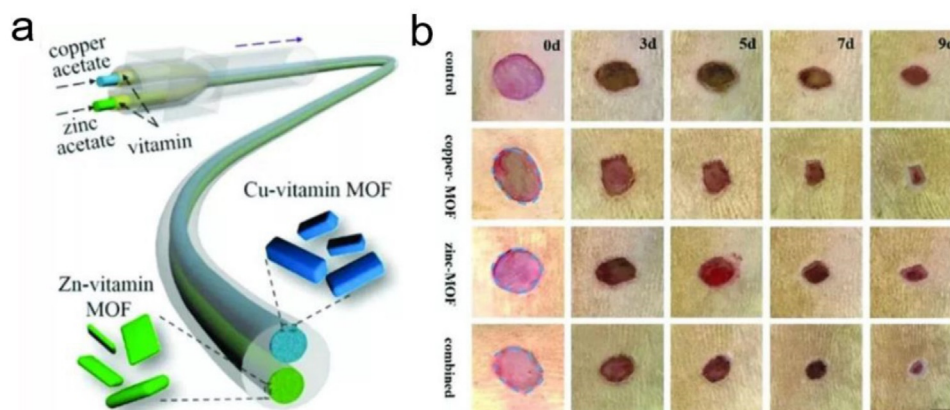


Fig. 18. (a) Schematic diagram of preparation of vitamin MOF hydrogel microfibers. (b) Photos of the skin wounds treated with Ca-Alg (control), copper-MOF microfibers, zinc-MOF microfibers, and combined MOF microfibers. The scale bar is 500 mm. The scale bar is 1 mm. Reproduced with permission [54]. Copyright 2018 The Royal Society of Chemistry.

centrations. It is obvious that the release of doxorubicin can be controlled by adjusting the concentration of ATP. Besides, as the ATP concentration increases, the release is gradually increased. As shown in Fig. 17c, only ATP can stimulate the selective release of doxorubicin from polyacrylamide/DNA-hydrogel coated MOFs, while other four kinds of nucleoside triphosphates are ineffective. Finally, as shown in Fig. 17d, polyacrylamide/DNA-hydrogel coated MOFs release a higher amount of doxorubicin under ATP triggering with less leakage than nucleic acid-terminated MOFs. This conclusion is obtained by comparing time-dependent amounts of doxorubicin released/leakage from polyacrylamide/DNA-hydrogel coated MOFs and nucleic acid-terminated MOFs. These results indicate that the report of polyacrylamide/DNA-hydrogel coated MOFs has successfully developed a high performance stimuli-responsive hydrogel-MOF nanoparticle as a drug carrier.

4.1.2. Wound healing

Chronic non-healing wounds remain a huge challenge and bring many unnecessary medical expenses [120]. However, copper ion might solve this issue because it is an important element of the human world and is involved in many processes related to wound healing because of promoting angiogenesis [121]. However, when copper ions are used for clinical treatment, it is necessary to expose the wound to copper salts or oxides multiple times, which would potentially expose the patient to excess toxic copper ions. In order to solve this thorny problem, copper ions were used as central ions to prepare a MOF material HKUST-1 [57]. Then, this material was embedded into a thermo-reversible citrate-based hydrogel with antioxidant. The composition of the hydrogel is poly-(polyethyleneglycol citrate-co-N-isopropylacrylamide), abbreviated as PPCN. This operation reduced the toxicity of copper ions and promoted wound healing. HKUST-1 did not destabilize the network of PPCN by shielding positive charges of copper ions. PPCN protected HKUST-1 from the disintegration through diffusion-limited degradation. This synergistic effect allowed the HKUST-1-PPCN composite to possess the advantages of both HKUST-1 and PPCN. Besides, HKUST-1 made the sustained release of copper ions possible, which can reduce the cytotoxicity of copper ions. The preserved antioxidant properties of PPCN can promote the cell migration, angiogenesis, collagen deposition, and accelerate the wound healing.

As shown in Fig. 18a, Zhao and coworkers used a coaxial capillary microfluidic system with multi-stage injection channels for continuous microfluidic spinning to prepare microfibers with alginate hydrogel as the shell and copper-vitamin or zinc-vitamin MOF as the core [54]. They also prepared microfibers containing two cores and three cores. The composition of the hydrogel microfibers can be precisely controlled since the concentration of the different components or pre-gel solutions can be used. The size of the hydrogel microfibers was also controllable by adjusting the flow rate of the microfluids. Due to the presence of the adjustable alginate hydrogel shell, the release process of the vitamin MOF hydrogel microfiber was mild and controllable. To validate the use of this vitamin MOF hydrogel microfiber in biomedical applications, Zhao and coworkers first tested its biocompatibility. As the concentration of metal ions increased, the cytotoxicity of the material gradually increased. Interestingly, there was a small increase in cell viability at very low metal ion concentrations, which may be the result of a combination of metal ions and vitamins. Subsequently, the antibacterial activity of vitamin MOF hydrogel microfibers and the ability to promote wound healing were tested. With the increase of copper ion concentration, copper-vitamin MOF hydrogel microfiber can effectively reduce the survival rate of *Escherichia coli*, thus preventing bacterial infection in the environment. It was found through experiments that biocompatibility and antibacterial activity can be achieved when the copper ion concentration is 0.158 mM. In addition, zinc-containing zinc-vitamin MOF hydrogel microfiber protected cells from oxidative damage. Finally, zinc-vitamin and copper-vitamin MOF hydrogel microfibers were used for wound healing in animals to verify their utility in promoting wound healing. As shown in Fig. 18b and c, after 9 days of treatment with MOF microfibers, the wounds healed substantially, however, the control group healed longer. The combination of zinc-vitamin and copper-vitamin MOF hydrogel microfibers is faster than the healing rate of each individual one. These results demonstrated that the antibacterial and antioxidant functions of these MOF hydrogel microfibers do contribute to wound healing.

4.1.3. Sensing

Chemical sensing technology is a very popular research area [122–124]. The detection of specific substances in liquids or gases by specific sensing materials allows people to find them quickly

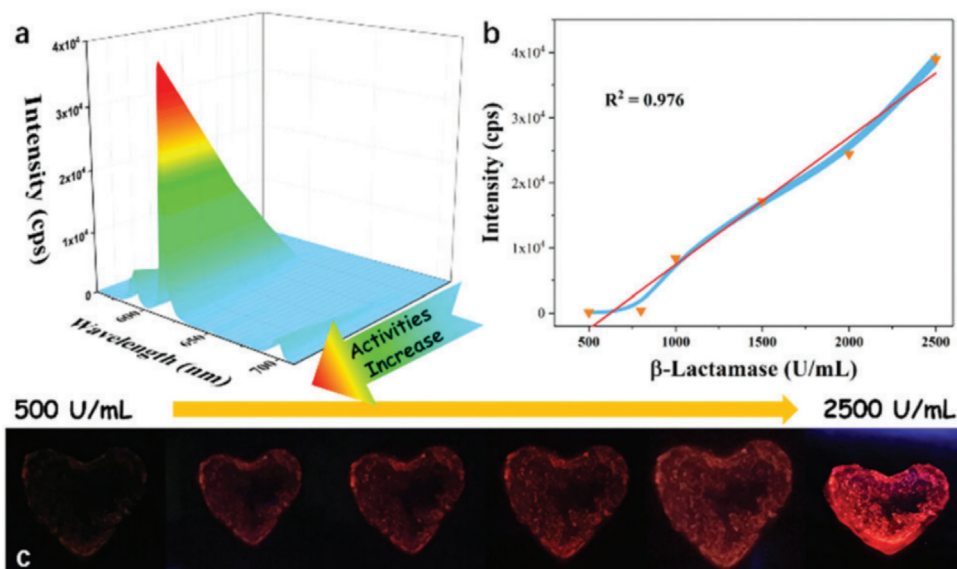


Fig. 19. (a) Luminescence responses of HM for the varying β -lactamase. (b) The relationship between intensities of HM and the concentrations of β -lactamase. (c) Photographs of the HM toward the various β -lactamase serum solutions with various concentrations. Reproduced with permission [62]. Copyright 2019 The Royal Society of Chemistry.

and easily [125]. In the face of the current serious health problems, exploring the application of new fluorescent or luminescent sensing materials for the detection of harmful substances in blood has always been one of the research hotspots in the fields of chemistry and materials [126]. In recent years, MOFs have attracted much attention in the field of fluorescent or luminescent sensing because of their unique advantages such as porosity, high specific surface area, and adjustable pore size [127–129]. At the same time, hydrogels have always been favored in the field of biosensing. Some work has been reported to combine these two materials for fluorescence sensing.

Penicillin is a β -lactam-based antibiotic that is a common drug against inflammation, but the use of penicillin is sometimes accompanied by poisoning and allergic reactions [130]. Therefore, the detection of the content of β -lactam in the blood of a patient using penicillin can effectively avoid the risk. A novel alginate hydrogel@MOF $[\text{Eu}_2(\text{BPDC})(\text{BDC})_2(\text{H}_2\text{O})_2]_n$ composite, named as HM, was used for β -lactam sensing [62]. The HM had high sensitivity and selectivity to β -lactam in both aqueous solution and serum. As shown in Fig. 19a, the luminescence signal of HM is positively correlated with the concentration of β -lactam. Fig. 19b shows the linear relationship between the intensity of luminescence signal and the concentration of β -lactam. After the sensing test, the β -lactam was irradiated with ultraviolet light. Fig. 19c shows that as the concentration of β -lactam increases, the color of HM under ultraviolet light changes from dark red to bright red. This indicates that the color of HM irradiated with ultraviolet light can intuitively reflect the resistance of patient to penicillin and diagnose the penicillin allergy.

Inorganic phosphate is an important electrolyte and is the key to maintain pH in human body [131]. Also, inorganic phosphate is involved in most metabolic processes and enzyme reactions. Therefore, the concentration of phosphate in the body affects the health of the human body. Sensing of different concentrations of phosphate is necessary. Based on a composite hydrogel consisting of a UiO-66- NH_2 , Rhodamine B (RhB, a fluorescent dye) and agarose hydrogel (as the matrix, a novel fluorescent sensing platform) were developed [52]. The porous structure of agarose facilitates the diffusion of phosphate in the hydrogel matrix. At 430 nm, the fluorescence intensity of UiO-66- NH_2 was sensitive to phosphate and increased with the increment of phosphate concentration. At 585 nm, a negligible change was observed for the fluorescence intensity of Rhodamine B. In the range of 0.5–10 mM, a good linear correlation was obtained between phosphate concentration and I430 nm/I585 nm. In addition, under the irradiation of ultraviolet light, the fluorescent color of the composite hydrogel also changed from orange to blue, which was consistent with the solution change. Besides, the use of composite hydrogel for the detection of phosphate in human serum has been applied. Emission spectra of composite hydrogels before and after incubated in serum samples indicated that a fluorescence color change was occurred. This sensing method is reliable, and can realize the visual measurement of the phosphate content in the serum of the human body, and is convenient for rapid detection.

Although these studies on sensors have shown excellent sensing performance of MOF-based hydrogels, their selectivity has not been highlighted. Obviously, selectivity is critical to the sensor. The composition of human blood is very complex, but also has individual differences. Therefore, how to improve the selectivity of these sensors in order to enhance their universality is an inevitable topic.

4.1.4. Water treatment

In daily life and in industrial production, various pollutants are discharged into the water environment [132]. At the same time, the usage of water resources is inevitable. Therefore, it is necessary

to develop useful techniques to remove pollutants from water. In the field of MOF-based hydrogels, some materials had been used to treat polluted water, and showed favorable practical potential.

Shi and coworkers attached the importance to process MOF particles into hydrogels, and proposed a one-step method to prepare a 3D alginate based Co-MOF hydrogel to remove tetracycline in water [63]. The microstructure of the as-synthesized Co-MOF-alginate hydrogel turned from a smooth surface into a particle-like face. It indicates that the Co-MOF-alginate hydrogel has a polymer skeleton and a whole Co-MOF structure. In tetracycline adsorption, the maximum adsorption capacity was 364.89 mg g^{-1} . After 10 cycles, the Co-MOF-alginate hydrogel had favorable regeneration properties. This report paved a novel way for preparing polymer based MOF hydrogels with potential for water treatment.

Maan et al. reported an *in situ* method to synthesize ZIF-8 in a polyacrylamide (PAM) hydrogel via using a zinc hydroxide PAM composite as the precursor gel [64]. They found the ability of this ZIF-8 PAM composite hydrogel to remove humic acid (HA) from water. This material possessed a maximum HA adsorption capacity of 111.5 mg g^{-1} ZIF-8 approximately, as shown in Fig. 20. The hydrogel showed improved adsorption efficiency for HA, and possessed easier synthesis operation than ZIF-8 powders.

4.2. MOF-based aerogels

Many scientific researches on MOF-based aerogels have been conducted because of their flexible processability, accessible specific surface areas, tunable pore sizes, excellent stability, and various properties. In this section, the studies of MOF-based aerogels in

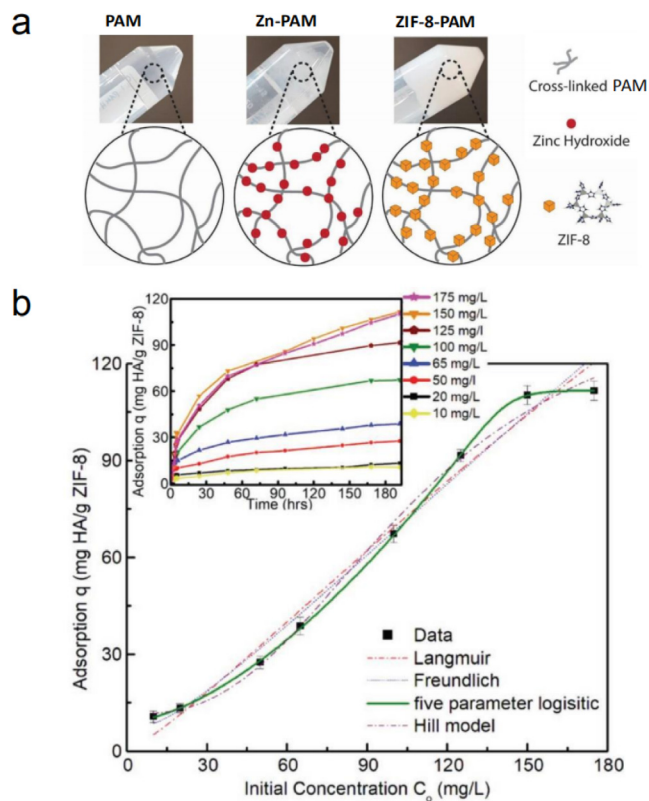


Fig. 20. (a) Schematic of the synthesis of ZIF-8 PAM hydrogel. (b) Effect of contact time and initial concentration of humic acid on the adsorption capacity of ZIF-8 PAM hydrogel for humic acid. Initial concentrations of humic acid range from 10 to 175 mg L^{-1} and contact time maximum was 7 days. Reproduced with permission [64]. Copyright 2019 Wiley-VCH Verlag GmbH & Co. KGaA, Weinheim.

applications including energy storage, adsorption, catalysis, and water treatment are discussed.

4.2.1. Energy storage

There has been fleetly growing scientific interest in electrochemistry applications such as in energy conversion and storage [133]. MOF-based aerogels have been utilized to be appropriate candidates in the field of electrochemistry. Furthermore, the rich porosity structures of MOFs are advantageous for fast mass transportation. The reports on MOF-based aerogels in electrical applications mainly involve lithium-ion batteries (LIBs) and supercapacitors.

4.2.1.1. Lithium-ion batteries (LIBs). The growing demand for advanced LIBs with large energy, power density, and long cyclic life in portable electronics has spurred forceful research efforts in the last few decades [134]. One of the most important cores of promoting the progress in LIBs lies in the research and development for safe and low-cost groundbreaking anode materials with desirable energy and power capabilities, such as metals and metal oxides. Metal oxides, such as MnO_2 , have gotten tremendous attention for high theoretical capacity and natural abundance [135]. However, as anode materials for LIBs, many common problems still exist for metal oxides and largely limit their electrochemical properties, including low rate capabilities and poor cycling stabilities result from large volume change and low inherent conductivity. To achieve satisfactory electrochemical performance, porous metal oxides have attracted interests because of their large surface area and high porosity. Porous architecture can provide shorter paths for speeding up the diffusion of Li^+ ions as well as electrons, and alleviate the volume change. In order to obtain porous metal oxide based aerogels, scientists pre-synthesize the MOFs in the surface of porous aerogels, such as 3D graphene, and then calcine the composites. Graphene aerogel matrix not only provides porous structure, but also greatly enhances the conductivity of the aerogel composites.

Zhang et al. prepared MIL-88-Fe derived $\text{Fe}_2\text{O}_3@3\text{D}$ graphene network ($\text{Fe}_2\text{O}_3@3\text{DGN}$) as the anode for LIBs. The 3DGN was served as current collector. In the first discharge curve of $\text{Fe}_2\text{O}_3@3\text{DGN}$ with good mechanical properties, the sloping voltage plateaus at 1.5 V can be attributed to the structural transformation of Fe_2O_3 and the sloping voltage plateaus at 1.0 V can be attributed to the insertion of lithium ions. The voltage plateau at 0.8 V was attributed to the reaction of $\text{Li}_2\text{Fe}_2\text{O}_3$ into Fe. This conversion was reversed in the charging process. Benefiting from its chemical composition, the $\text{Fe}_2\text{O}_3@3\text{DGN}$ composite exhibited a reversible capacity at 0.2 A g^{-1} of 864 mAh g^{-1} after 50 cycles, higher than that of Fe_2O_3 powder (261 mAh g^{-1}). Moreover, the rate capacities of $\text{Fe}_2\text{O}_3@3\text{DGN}$ exhibited 10th-cycle discharge capacities of 871, 785, and 587 mAh g^{-1} at current densities of 0.2, 1, and 5 A g^{-1} , respectively. In contrast, Fe_2O_3 electrode exhibited 10th-cycle discharge capacity of less than 50 mAh g^{-1} at current density of 1 A g^{-1} . $\text{Fe}_2\text{O}_3@3\text{DGN}$ with low areal density is promising for the industrialization of lightweight LIBs because of the reduced total weight and high capacity of per unit mass [118].

Porous $\text{Fe}_2\text{O}_3@$ three-dimensional graphene aerogel ($\text{Fe}_2\text{O}_3@3\text{DGA}$) was designed as an anode for LIBs. The capacity of $\text{Fe}_2\text{O}_3@3\text{DGA}$ (1129 mAh g^{-1}) at 0.2 A g^{-1} after 130 cycles was obviously better than that of $\text{Fe}_2\text{O}_3@3\text{DGN}$ (864 mAh g^{-1}) after 50 cycles. $\text{Fe}_2\text{O}_3@3\text{DGA}$ possessed outstanding cycling stability after 1200 cycles at 5 A g^{-1} with capacity retention more than 97%. Compared with $\text{Fe}_2\text{O}_3@3\text{DGN}$, $\text{Fe}_2\text{O}_3@3\text{DGA}$ had larger surface area and richer pore structure. Besides, porous Fe_2O_3 nanoparticles could be uniformly encapsulated in graphene aerogel, on the contrary, Fe_2O_3 were simply deposited on the surface of 3DGN. Especially, porous $\text{Fe}_2\text{O}_3@3\text{DGA}$ was used as flexible anode directly

for LIBs upon mechanical pressing, indicating that the preparation process of anode can be simplified [90].

Yuan et al. synthesized binder-free porous $\text{CuO}@3\text{DGN}$ anode via using solution immersion method and a subsequent thermal treatment. $\text{CuO}@3\text{DGN}$ possessed a reversible capacity of 409 mAh g^{-1} at 0.1 A g^{-1} and outstanding cycling stability after 50 cycles at 5 A g^{-1} with a capacity of 219 mAh g^{-1} at 1.6 A g^{-1} . The outstanding performance of the electrode can be attributed to the synergistic interaction between porous CuO with high capacity and the porous 3DGN with large surface area [117]. Moreover, they reported graphene aerogel encapsulated Fe-Co oxide nanocubes (Fe-Co oxide@GA). The Fe-Co oxide nanocubes were derived from Prussian Blue Analogue (PBA) as self-sacrificial template. The Fe-Co oxide@GA composite was used as integrated anode material in lithium-ion batteries. The anode material possessed an excellent cycle stability with a specific capacity of 947 mAh g^{-1} at 100 mA g^{-1} after more than 100 cycles. The interconnected network of GA provided the space for buffering volume change of Fe-Co oxide. Contrarily, Fe-Co oxides strongly wrapped within GA contribute large specific capacity [136].

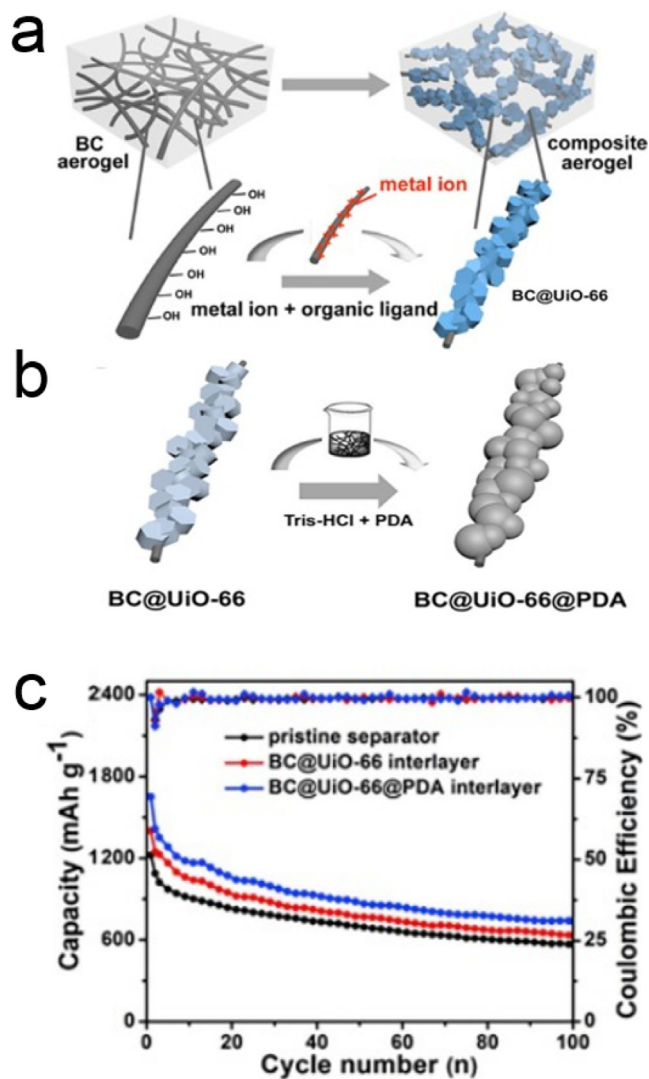


Fig. 21. (a) The fabrication process of bacteria cellulose @MOFs composite aerogels ($\text{BC}@UiO-66$). (b) The fabrication process of $\text{BC}@UiO-66@PDA$. (c) The cycling stability/retention and corresponding coulombic efficiency of lithium-sulphur battery with pristine separator, $\text{BC}@UiO-66$ interlayer and $\text{BC}@UiO-66@PDA$ interlayer at 0.5C. Reproduced with permission [137]. Copyright 2019 Elsevier Inc.

As shown in Fig. 21a and b, a bacteria cellulose (BC)@UiO-66 nanofiber aerogel was designed. It had a high reversible capacity of 631 mAh g^{-1} at 0.5 C after 100 cycles as a flexible lithium-sulfur battery interlayer film. It should be attributed to the preeminent selectivity for Li^+ ions and efficient inhibition to the soluble polysulfide ions. Moreover, the presence of polydopamine (PDA) coating on BC@UiO-66 nanofiber aerogel increased the reversible capacity to 739 mAh g^{-1} at 0.5 C over 100 cycles (Fig. 21c) [137].

4.2.1.2. Supercapacitors. Supercapacitor is a new type of energy storage devices between traditional capacitors and rechargeable batteries, which mainly depends on double layer and redox pseudo-capacitor charge [138]. Different from traditional electrochemical power source, supercapacitor is a kind of power sources between traditional capacitors and batteries. It has the advantages of high power density, short charge as well as discharge times, long cycle life, and wide working temperature range [139]. Therefore, supercapacitors, especially flexible supercapacitors, have great application value and market potential in many fields, such as industrial control, electric power, transportation, intelligent instrument, national defense, new energy vehicle, and so on. The performance of supercapacitors is dependent on surface area and electrical conductivity of electrode materials [140]. Recently, MOF-based aerogels have been investigated in supercapacitor applications because of porous structures and convenient preparation methods. Besides, MOF-based aerogels are able to provide effective contact between the electrolyte and electrodes. For instance, $\text{Fe}_2\text{O}_3/\text{rGO}$ composite aerogel, prepared by calcinating a mixture of Fe-MOF crystals and GO, showed an ideal rate capability behavior with high specific capacitance of 869.2 F g^{-1} and at the current densities of 1 A g^{-1} and 289.6 F g^{-1} at the current densities of 20 A g^{-1} , respectively [91]. Liu et al. designed a graphene assisted method to break bulk Co-based MOF ($\text{Co}(\text{mIM})_2$

($\text{mIM} = 2\text{-methylimidazole}$)) crystals into porous carbon combined with N-doped graphene aerogel, represented by C@NGA composite. After removing of Co from the composite, it was used as the electrode in supercapacitor. In the $1 \text{ M H}_2\text{SO}_4$ solution, all CV curves exhibited semirectangular shapes from -1.0 to 0 V (vs Ag/AgCl). The current response increased when increasing the scan rate, indicating excellent rate capability of C@NGA. All of the galvanostatic charge-discharge (GCD) curves displayed typical triangular profiles. C@NGA exhibited 421 F g^{-1} capacitance at the current density of 1 A g^{-1} . C@NGA possesses excellent cycling stability after 20,000 cycles with a capacitance retention more than 99% (Fig. 22) [93].

Remarkably, by changing the addition order of Fe^{3+} ions, the MOF composites on graphene will evolve different morphologies and crystal structures. One of them was the oriented rod-like MIL-88-Fe growing at (0 0 2) lattice plane on the surface of graphene (rod-like MOF@GA), and another was the spindle-like MOF dispersing on the graphene surface (spindle-like MOF@GA). As the materials for supercapacitors, the capacitance of GA with MIL-88-Fe can be improved by introducing the MIL-88-Fe. The capacitance of spindle-like MOF@GA was about 353 F g^{-1} at the scan rate of 20 A g^{-1} . Besides, rod-like MOF@GA had higher capacitive volume, faster charge/discharge rate, and more reliable cycling stability than spindle-like MOF@GA. The oriented MOFs (rod-like MOFs) on graphene sheets can promote the capacitive capability via using the mesopores and macropores of GA, which can provide channels for ion transportation. After 10,000 cycles testing, the retention ratio can reach 74%. This study reveals that the morphology and growth patterns of MOFs on aerogels matrix greatly affect their properties [83].

Qu and coworkers synthesized NiS nanorods (derived from Ni-MOF-74)-modified reduced GA as an electrode [141]. The electrode displayed excellent specific capacity of 744 C g^{-1} at 1 A g^{-1} and

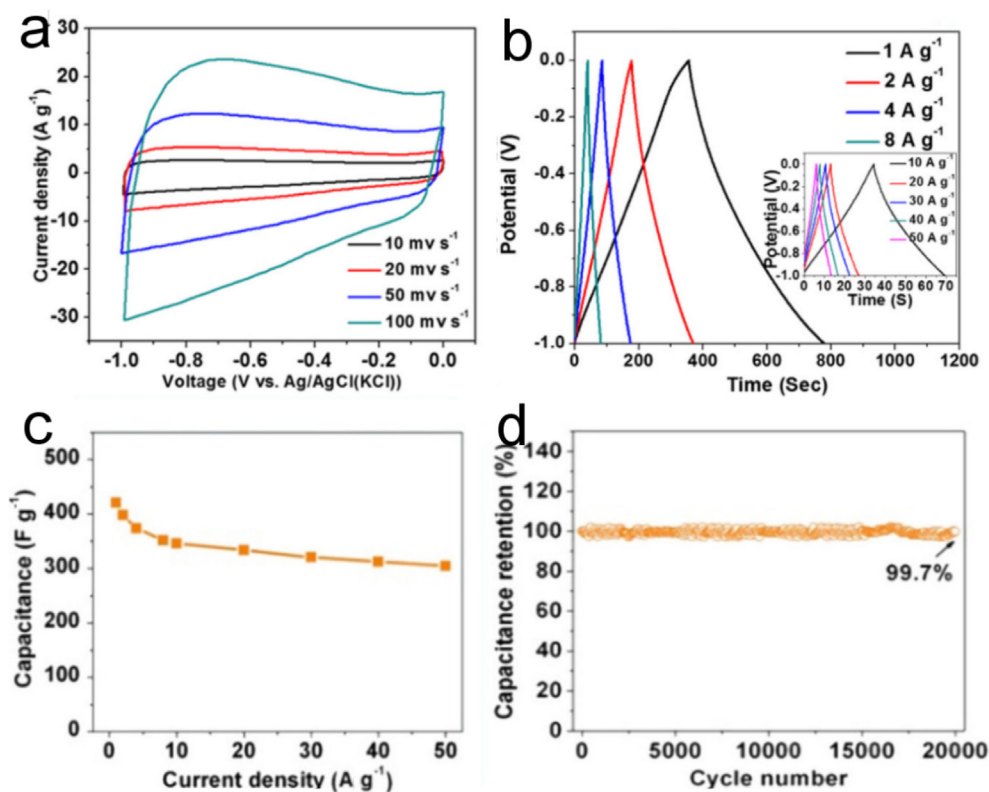


Fig. 22. (a) The CV curves of C@NGA at various scan rates in H_2SO_4 solution. (b) GCD curves of C@NGA at various current densities. (c) The specific capacitance of C@NGA. (d) The cycling stability of C@NGA at 20 A g^{-1} . Reproduced with permission [93]. Copyright 2017 American Chemical Society.

600 C g⁻¹ at 50 A g⁻¹ and excellent cycle life after 20,000 cycles. The performance was better than other nickel sulfide-based electrodes. The enhanced performance should be attributed to the active (1 1 0) and (1 0 1) edges of the hybrid. These edges exhibited a forceful affinity for OH⁻ in KOH electrolyte. Then a hybrid supercapacitor based on them was constructed by coupling this hybrid to the capacitive electrode. The as-designed device possessed extraordinarily high energy and power densities.

4.2.2. Catalysis

As typical catalysts, MOFs have the following advantages: (1) the selectivity from the shape and size of the porosity and (2) the diversity of functional groups [142,143]. Among the functional applications of MOF-based aerogels, catalysis is one of the most rapidly developing fields. There are high densities and uniform dispersive catalytic activity sites in the structures of MOF-based aerogels. Their pore structures ensure the accessibility of every catalytic active site. The large pore channels of aerogel matrixes greatly facilitate the transport of substrate and products from catalytic reactions.

4.2.2.1. Electrocatalysis. The working mechanism of fuel cell, a promising technology for generating electricity, mainly includes two half reactions: fuel oxidation and oxygen reduction [144]. In general, the rate of oxidation reaction is faster than that of reduction reaction, so it is very important to increase the rate of oxygen reduction reaction (ORR). The common catalyst to accelerate the ORR is commercially-available Pt/C, however, it is urgent to explore alternative materials due to the high price of Pt [145].

Fe-2,2'-bipyridine-3,3'-dicarboxylic acid-C₃N₄-carbon aerogel (Fe-bpdc-C₃N₄-CA) was synthesized by H. Zhu and coworkers. The Fe-bpdc MOF and g-C₃N₄ were encapsulated into a resorcinol-formaldehyde resin to obtain a composite, and then, the composite was crushed by ball milling method and carbonized by calcination to get Fe-bpdc-C₃N₄-CA. The doping of N heteroatoms was critical

to ORR, and Fe-N_x active sites had good catalytic activity for ORR. The presence of porous carbon aerogel ensured the conductivity of the composite. Fe-bpdc-C₃N₄-CA catalysts exhibited stable ORR activity with initial reduction potential (1.09 V) and half-wave potential (0.96 V) vs reversible hydrogen electrode (RHE) in 0.1 mol L⁻¹ KOH [146].

In addition, some MOF-derived metal oxides also play an important role in the field of electrocatalysis combined with N-doped GA. Zou et al. made [Fe₃O(H₂N-BDC)₃] (H₂N-BDC = 2-aminoterephthalic acid, denoted as MIL-88B-NH₂) grow on the surface of the pre-synthesizing nitrogen-doped graphene hydrogel. After solvent exchange, freeze drying and pyrolyzation, Fe₃O₄@nitrogen-doped graphene aerogel (named as Fe₃O₄@NGA) was obtained. The Fe₃O₄ nanoparticles with rich edge area in aerogel supported considerable active sites for ORR. Compared with Pt/C, Fe₃O₄@NGA possessed more satisfied ORR catalytic activity (high onset potential (0.92 V) and peak potential (0.77 V) vs RHE in O₂-saturated 0.1 mol L⁻¹ KOH), as well as longer term durability (After 500 min, 65% of the relative current density can be retained) [92].

Cui et al. reported a cobalt-embedded nitrogen-doped GA (Co-N-GA) pyrolyzed from a MOFs@GA composite, and used it as a catalyst for ORR (Fig. 23a). As shown in Fig. 23b and c, the porous catalyst possessed a high surface area (466.6 m² g⁻¹) and hierarchical porosity, including macropores, mesopores, and micropores. Owing to the synergetic effect of hierarchical porosity and high surface area, Co-N-GA displayed superior activity for ORR with excellent stability in 0.1 mol L⁻¹ KOH. Fig. 23d-i indicates that the ORR activity, durability, and selectivity of Co-N-GA were superior than commercial Pt/C, indicating its advantages of practical applications [94]. In addition, this material also has a good performance in hydrogen evolution reaction (HER). The onset overpotential was 0 mV, the overpotentials@10, 100 mA cm⁻² were 46 mV, 183 mV, respectively, and Tafel slope is 33 mV dec⁻¹. These values are lower than almost all as-prepared noble-metal-free HER

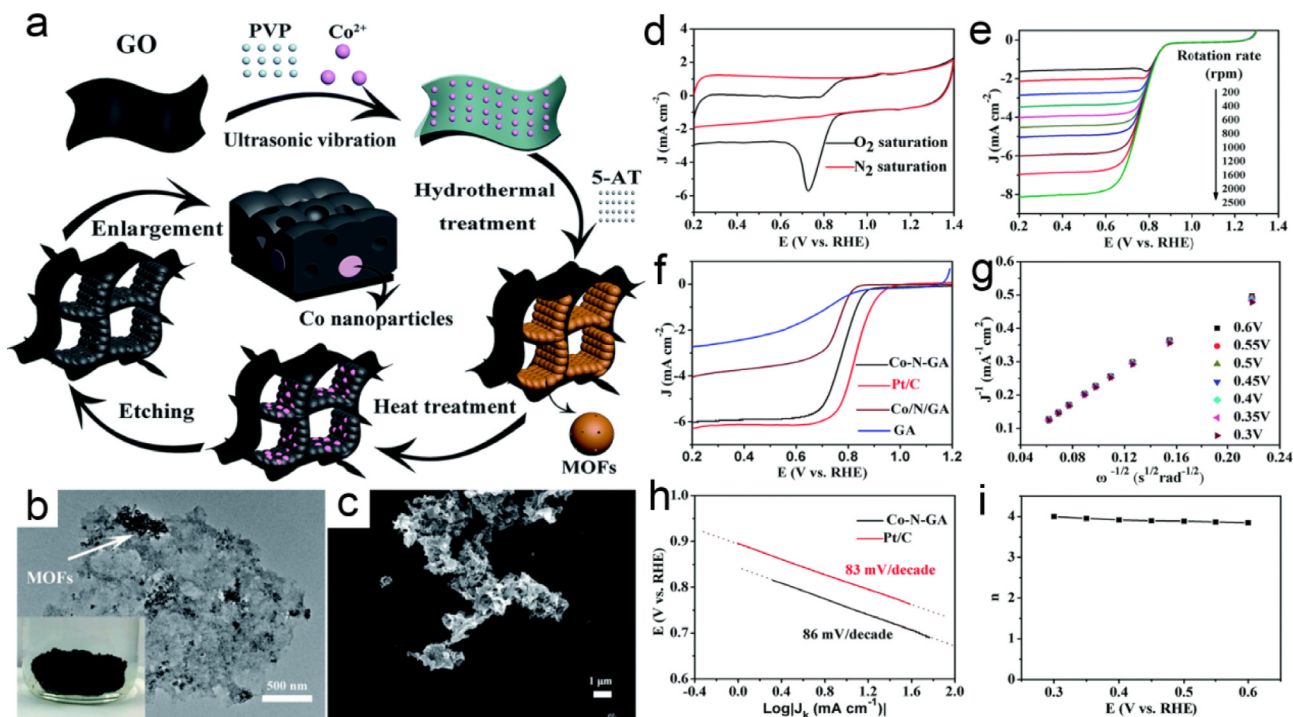


Fig. 23. (a) The preparation process of Co-N-GA. (b) The typical TEM of Co-N-GA; the inset shows the typical photograph of Co-N-GA. (c) The typical SEM of Co-N-GA. (d) The CV curves of Co-N-GA in N₂-saturated and O₂-saturated KOH solution with 0.1 M concentration. (e) ORR polarization curves at 10 mV s⁻¹ at 1600 rpm. (f) Corresponding Tafel plots of Pt/C and Co-N-GA. (g) ORR polarization curves of Co-N-GA (different rotating speeds at 10 mV s⁻¹). (h) K-L plots of Co-N-GA at different potentials. (i) The electron transfer numbers of Co-N-GA at various potentials based on K-L data. Reproduced with permission [94]. Copyright 2016 The Royal Society of Chemistry.

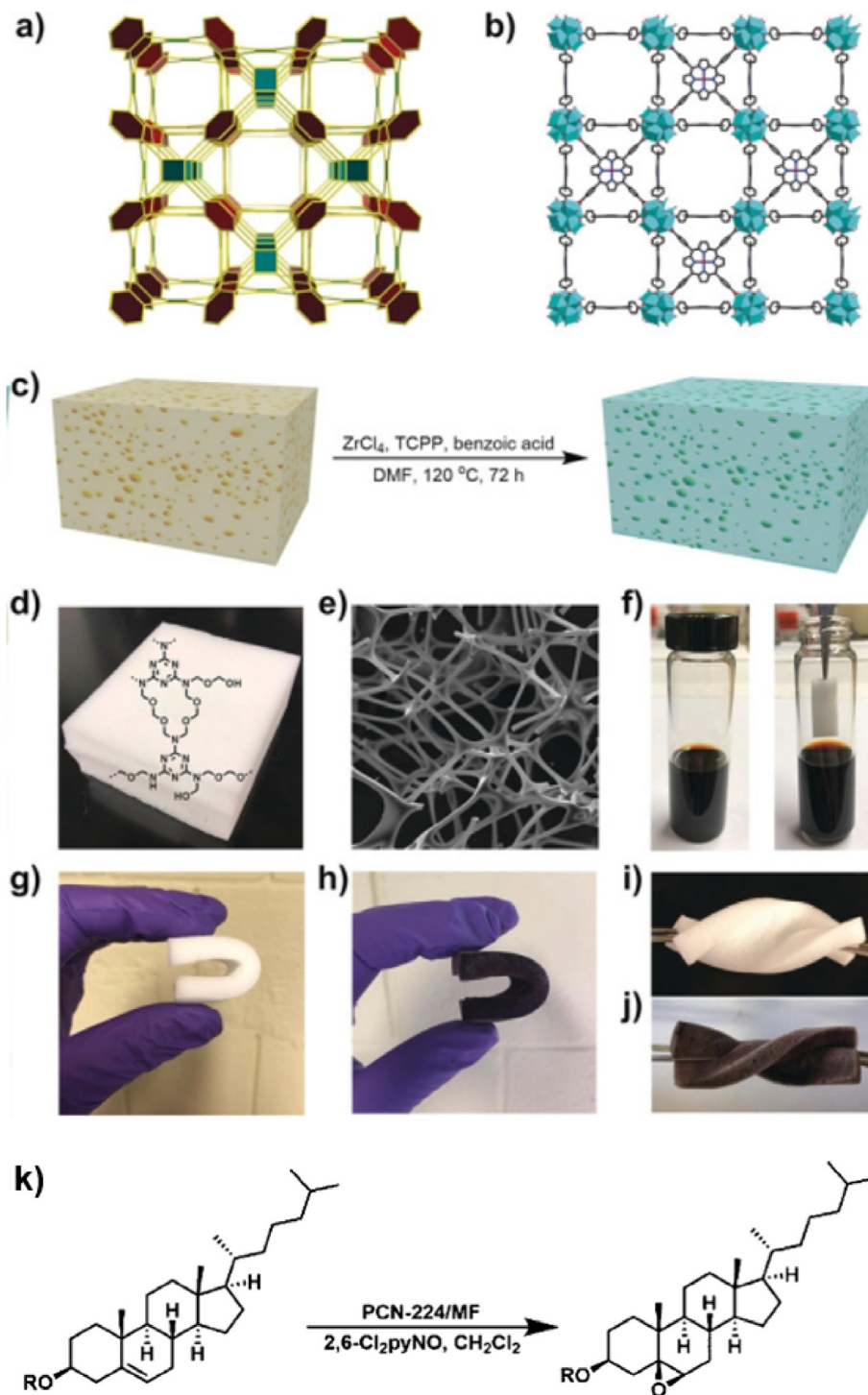


Fig. 24. (a) The topological structure of MOF PCN-224. (b) View down the tetragonal channels of MOF PCN-224 (C atom, black; M atom, purple; N atom, blue; hydrogen omitted). (c) The procedure for the preparation of the MOF PCN-224 decorated melamine foam composites. (d) Photograph of melamine foam and its chemical formula. (e) The typical SEM image of the melamine foam. (f) A mixture of tetrakis (4-carboxyphenyl)-porphyrin (Fe), $ZrCl_4$, and benzoic acid in DMF solution (left) and immersing the melamine foam into the solution (right). (g) Photograph of melamine foam. (h) Photograph of PCN-224@MF. (i) The melamine foam could be compressed and distorted. (j) The PCN-224@MF could be compressed and distorted. (k) The epoxidation reaction of cholesteryl esters by using PCN-224@MF as the catalyst. Reproduced with permission [150]. Copyright 2018 Wiley-VCH Verlag GmbH & Co. KGaA, Weinheim.

catalysts, which indicates that this material possesses excellent activity for HER. Notably, the Co-N-GA displayed favorable stability for HER in acidic and alkaline media. The stability should be attributed to the fact that 3D graphene aerogel architecture possesses strong chemical stability in a harsh environment.

Overall, the research on electro-catalysis of MOF-based aerogels mainly focuses on ORR, while more other catalytic forms such as HER are required to be conducted in the future. Besides, the electro-catalytic performances of MOF-based aerogels are satisfactory. However, in terms of absolute catalytic performance, there is

still a gap with some materials such as bimetallic materials [147,148]. It may be meaningful to try to composite some monometallic or bimetallic nanoparticles with small size in MOF-based aerogel structure and explore their catalytic activity.

4.2.2.2. Other catalysis. Heterogeneous catalysis is very popular in the field of organic chemistry. Compared with homogeneous catalysts, heterogeneous catalysts have the advantages of easy separation of products, recoverability, and less metal loss [149]. As novel heterogeneous catalysts, the catalytic activity sites of MOF-based aerogels can be derived from metal ions or organic ligands. MOF-based aerogels, which possess low density, excellent mechanical capacity, good stability, can provide different reaction spaces for reactants.

By catalytic epoxidation, unsaturated cholesteryl esters have the potential to produce certain cholesterol derivatives, which act as sanatory medicines for diseases. By using a one-pot strategy, Zhou et al. integrating MOF PCN-224 (PCN-224 is constructed with tetrakis (4-carboxy-phenyl)-porphyrin ligands and Zr_6 clusters) and porous melamine foam (MF) into composite, named PCN-224@MF (Fig. 24a–j). PCN-224@MF possessed high efficiency in the epoxidation of *cis*-stilbene (Fig. 24k). Encouraged by this property, this material was used for catalyzing epoxidation reaction of cholesteryl esters from unsaturated cholesteryl. Under the most appropriate condition, an excellent yield (92%) of corresponding product was obtained after one day because of the macroporous structures of MF and dispersedly distributed catalytic active sites of PCN-224 [150]. Based on porous MF, chemists can synthesize more composites used in heterogeneous catalysis by changing the types of metal ions and ligands.

Martyanov et al. prepared HKUST-1@silica aerogel composite pellets by applying the coupled sol-gel and emulsion methods for catalyzing styrene oxide to phenyl acetaldehyde. The conversion of styrene oxide at 110 °C was more than 85% and the selectivity to phenyl acetaldehyde was 93% in a flow reactor under nitrogen. Notably, when the time-on-stream reached 90 min, the conversion was more than 50%, and the selectivity was not changing visibly, indicating the application potential of HKUST-1@silica aerogel composite pellets in continuous flow catalysis [78]. Martyanov et al. found that the characteristic X-ray diffraction (XRD) peaks of the recycled HKUST-1@silica aerogel composite pellets after catalytic testing were not different from the peaks of original HKUST-1@silica aerogel composite pellets. It indicates the excellent stability of the HKUST-1 crystal structure during the catalytic reaction.

Lu et al. employed Ru/GA-HKUST-1 for the oxidation of carbon monoxide (CO). The CO conversion ratio (100%) of Ru/GA-HKUST-1 was higher than that of the Ru/GA without HKUST-1 (19.8%) at 30 °C, because the open porous structures of HKUST-1 provided pathways for adsorption and catalytic oxidation simultaneously [84]. This interesting finding provides a feasible strategy for enhancing the adsorption capacity of reactants around the catalyst and increasing the catalytic reaction rate.

4.2.3. Water treatment

Water treatment refers to the physical and chemical measures taken to make the water quality meet certain use standards [151]. There are many kinds of harmful substances in water, and the relative treatment methods are different. The treatment can be classified as degradation and adsorption. MOF-based aerogels have abundant pore structures and are favorable for adsorption [152]. Metal ions in MOF can also provide active sites for the degradation of harmful substances [153]. Crucially, these MOF-based aerogels can be easily removed from aqueous solutions for reuse after the previous water treatment process, which is fascinating. Therefore, MOF-based aerogels are widely used in water treatment.

4.2.3.1. Pollutants degradation. The degradation of harmful organic pollutants via catalytic methods is necessary. P-nitrophenol (PNP) is flammable, toxic and allergic to the skin. In order to degrade PNP, we loaded ZIF-9 and ZIF-12 (Fig. 25a) on cellulose aerogels to convert peroxymonosulfate (PMS) into sulfate radicals ($SO_4^{\cdot-}$), which plays the key role in PNP degradation, as shown in Fig. 25b. The two hybrid aerogels, combined with activated PMS, could remove more than 80% of PNP in 60 min. The green aerogel composites can be easily separated from the treated solution and possesses good recyclability [88].

It is interesting to note that there are some MOF-based aerogels that can rely on more than one catalytic mode for synergistic effect. For example, MOF (2Fe/Co)@carbon aerogel (CA) with appropriate electrocatalytic and photocatalytic activity was applied in solar photo-electro-Fenton (SPEF) process for removing Rhodamine B (100%) and dimethyl phthalate (85%). MOF (2Fe/Co) promoted the ORR activity and improved the yield of H_2O_2 . Simultaneously, the photoinduced electron (ecb^-) of MOF (2Fe/Co) instantly reacted with H_2O_2 to improve the generation of $\cdot OH$ radicals, which could react with organic pollutants and obtain carbon dioxide and water. In the pH range of 3–9, MOF (2Fe/Co)@CA retained ideal degradation efficiency [154].

4.2.3.2. Liquid adsorption. Industrial liquid wastes always contain a certain concentration of hazardous heavy metal ions and organics, which will pollute the water and environment and endanger human health. Therefore, it is urgent to eliminate hazardous substances from industrial wastewater [155,156]. In addition, some contaminated fresh water sources are in urgent need of decontamination to reclaim clean fresh water resources [157].

To date, scientists have developed many materials to adsorb harmful substances and contaminations in water. Cr (VI) is an ingestion poison or an extremely toxic inhaled substance [158]. Exposing skin to Cr (VI) may lead to genetic defects. People who drinking contaminated water containing Cr (VI) ion may suffer

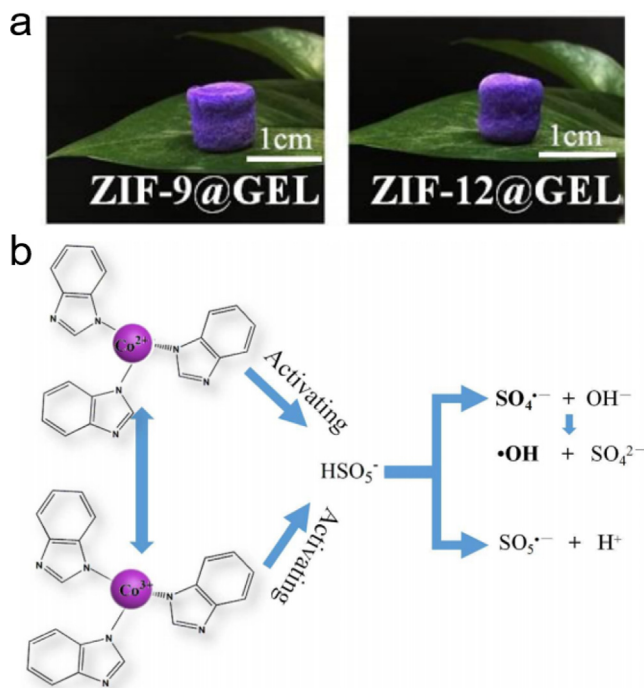


Fig. 25. (a) Photos of the synthesized hybrid aerogels containing ZIF-9 and ZIF-12. (b) The mechanism schematic of MOF@GEL/PMS system to generate free radicals. Reproduced with permission [88]. Copyright 2018 Elsevier Inc.

from cancer [159]. UiO-66@cellulose aerogel with tunable MOF loading was prepared to adsorb Cr (VI) ion in water, because the hierarchical porous structure of aerogel allows the fast uptake and reaction between Cr (VI) ion and UiO-66. The water containing Cr (VI) ion was initially yellow but became colorless after adding the UiO-66@cellulose aerogel. At the same time, the color of the aerogel changed from white to yellow. The aerogel with 50 wt% UiO-66 loadings can adsorb 85% of the Cr (VI) ion in water after 24 h, but aerogel containing 33.3 wt% UiO-66 can adsorb 67% of the Cr (VI) because of the low MOF content. After adsorbing Cr (VI) ion with low concentration, the aerogel can be compressed to squeeze out the adsorbed water, then adsorb the bulk solution containing higher concentration of Cr (VI) ion [87]. Our group reported that ZIF-8@cellulose aerogel possessed Cr (VI) ion adsorption potential. Fig. 26 shows the morphologies of ZIF-8, cellulose aerogels, and ZIF-8@cellulose aerogel. The high binding potential, high specific surface area and superior processability endowed this ZIF-8@cellulose aerogel possess high adsorption capacity towards Cr (VI) ion. The removal rates of Cr (VI) ion by ZIF-8@cellulose aerogel were higher than 90% in all concentration ranges (1 ppm to 100 ppm), which were higher than that in UiO-66@cellulose aerogel. Importantly, when the initial concentration of Cr (VI) ion was 1 ppm, ZIF-8@cellulose aerogel could remove 99.74% of Cr (VI) ion from the contaminated water, being among the top rank of Cr (VI) ion adsorption in chemical materials [160].

Besides, our group also reported an *in situ* growth procedure to load MOFs (UiO-66-NH₂ and UiO-66) on the flexible cellulose aerogels as aerogels composite materials. These materials were favorable Pb²⁺ and Cu²⁺ adsorbents. The MOFs were not blocked after cellulose aerogels growth, so UiO-66-NH₂@cellulose and UiO-66@cellulose aerogels can be recycled to adsorb the above-mentioned two ions in water after cleaning. The equilibrium adsorption capacity of Pb²⁺ ion adsorbed by UiO-66-NH₂@cellulose aerogel was 89.40 mg g⁻¹, and the equilibrium adsorption capacity of Cu²⁺ ion was 39.33 mg g⁻¹ [161].

Printing and dyeing companies usually need to use large amounts of freshwater resources and drain the contaminated water containing dyes such as Rhodamine B (RhB), Methyl Orange (MO), Malachite Green (MG), Crystal Violet (CV), Congo Red (CR) and Brilliant Blue R-250 (BBR-250) into the environment [162–166]. At present, since fresh water resources are very precious, it is very meaningful to regenerate contaminated water by adsorbing dyes. Li et al. reported that the maximum adsorption capacity of ZIF-8@fibrous aerogel for RhB dye could be up to 81 mg g⁻¹ [167]. Besides, ZIF-67@GA not only adsorbed RhB dye but also MO dye. The adsorption ability of ZIF-67@GA towards MO dye was larger than that of RhB dye, because ZIF-67@GA reacted differently with two dyes. Owing to the electrostatic attraction, ZIF-67 with positive surface charge can enhance the retention anionic MO dye in the ZIF-67@GA. In contrast, ZIF-67@GA absorbed cationic RhB dye by weak π - π interaction between grapheme and RhB [168]. Yang and coworkers have reported similar research about adsorb CV dye and MO dye by using ZIF-67@rGA. The maximum

adsorption capacity was 1714.2 mg g⁻¹ for CV dye and 426.3 mg g⁻¹ for MO dye (Fig. 27). The adsorption towards cationic CV dyes was driven by π - π interactions, as well as electrostatic interactions between ZIF-67@rGA and CV dye [169]. Su et al. achieved a synthetic route to fabricate porous Al (III)-carboxylate aerogel that featured high surface area, tunable porosity and low density to absorb dyes. The aerogel displayed a fast uptake of CR and BBR-250 dye molecules. The adsorption capacities reached 633.4 mg g⁻¹ for CR and 621.3 mg g⁻¹ for BBR-250, because the mesopores of Al (III)-carboxylate aerogel were accessible to dye molecules and facilitated the adsorption [74]. In addition, owing to the π - π interaction between ZIF-67 and MG, ZIF-67@melamine sponge showed the highest adsorption capacity to date for toxic MG dye of 4093 mg g⁻¹. In this study, ZIF-67@melamine sponge could be regenerated effectively by washing it with ethanol and reused for absorbing MG dye. After three cycles of washing, ZIF-67 nanocrystals remained stable on the melamine sponge [170]. The excellent regeneration greatly enhances the commercial potential of ZIF-67@melamine sponge.

The removal of other organics from water also has been studied. A Zr-MOF@GA was synthesized and used to remove hydroquinone after the immobilization of laccase with adsorption rate of 73.8 mg g⁻¹. Owing to the combination of GA adsorption and the catalysis by laccase attached to Zr-MOF, the composite removed 79% of hydroquinone [171]. ZIF-8@konjac glucomannan (KMG) aerogel was prepared for the removal of ciprofloxacin (CIP) from water. Electrostatic attraction between CIP and ZIF-8@KMG aerogel played the most critical role in CIP adsorption. When the ratio of KGM to ZIF-8 was 1.4, the CIP adsorption capacity reached to the maximum (more than 920 mg g⁻¹). However, when the content of ZIF-8 further increased, the adsorption capacity decreased, because the excessive content of ZIF-8 led to unstable structure that was prone to collapse [99]. It is indicating that the adding amount of MOFs in aerogel matrixes should be carefully studied because this research has a great impact on the application performance of aerogel composites.

Li and coworkers grew Ni/Co-MOF in the pores of the CMC aerogel to synthesize a novel aerogel composite named as Ni/Co-MOF@CMC aerogel [100]. The aerogel composite can remove tetracycline hydrochloride (TC) within 5 min. The removal efficiency was 80% approximately, and the adsorption capacity was 624.87 mg g⁻¹ approximately. The adsorption mode between TC and Ni/Co-MOF@CMC aerogel was chemisorption. Because of the hydroxyl groups and carboxy groups in CMC aerogel, it is unnecessary to modify this aerogel to form a solid MOF film. The TC molecules in solution were more likely to contact with compact MOF layer during the solution flowing through the aerogel composite, which was necessary for removing TC. Besides, the as-prepared Ni/Co-MOF@CMC aerogel showed excellent antibacterial properties. This aerogel composite can be used for efficient and recyclable water treatment.

Some aerogels have a wide range of applications and can absorb a large number of liquid contaminants. Ma and coworkers reported

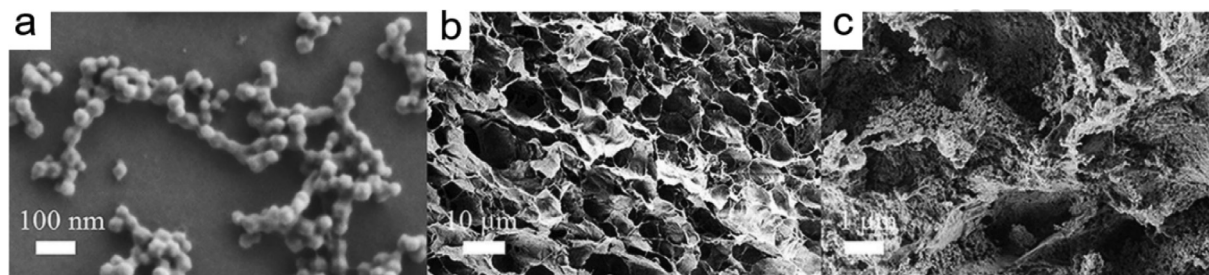


Fig. 26. (a) SEM image of ZIF-8. (b) SEM image of cellulose aerogels. (c) SEM image of ZIF-8@cellulose aerogel. Reproduced with permission [160]. Copyright 2018 Elsevier Inc.

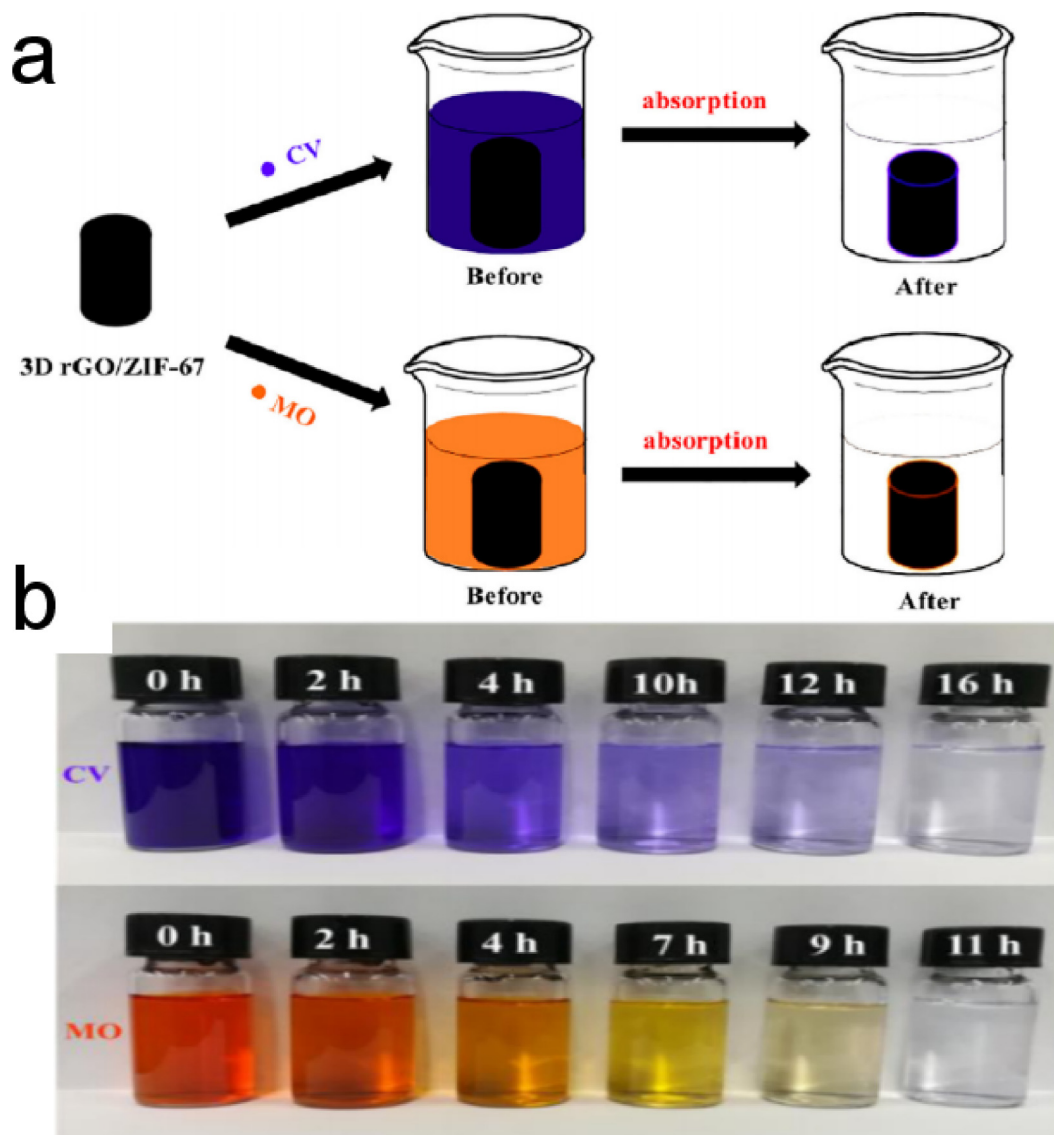


Fig. 27. (a) The scheme of removal process of CV and MO by ZIF-67@rGA. (b) The photographs of CV and MO solution at different adsorption time. Reproduced with permission [169]. Copyright 2018 Elsevier Inc.

a lightweight porous ZIF-8@cellulose nanofiber@cellulose foam (ZIF-8@CNF@cellulose) with outstanding adsorption properties. The ZIF-8@CNF@cellulose showed high adsorption capacity for 24.6 mg g^{-1} RhB dye, 35.6 mg g^{-1} Cr (VI) ions and 45.2 g g^{-1} N,N-dimethylformamide (DMF) [172].

The above-mentioned studies indicate that the unique pore structure of MOFs and the stability of aerogels contribute to the development of reusable water treatment materials. The microporous structure of MOFs combined with the diversity of ligands and metal ions enables them to adsorb different kinds of harmful substances in water. At the same time, aerogel solves the problem that single MOF material cannot be recycled and reused. In general, the use of MOF-based aerogels for efficient water treatment is a new and far-reaching area. With the further improvement of the preparation process, the industrial application will be obtained in the near future.

4.2.4. Gas adsorption

The permanent porosity, high specific surface area, and multitudinous functionalization make MOF-based aerogels conventionally used in gas adsorption. Compared with MOFs powders, the

better recyclability and portability of MOF-based aerogels enhance their application value of gas adsorption.

Stimulated by global warming, which is the result from the increased CO_2 emission, the adsorption of CO_2 is becoming important [173]. Well-designed ZIF-8@GA with a pore volume of $0.67 \text{ cm}^3 \text{ g}^{-1}$ and a BET surface area of $1099 \text{ m}^2 \text{ g}^{-1}$ was prepared, and then checked for the CO_2 adsorption application. The incorporation of ZIF-8 into GA matrix resulted in an increase of CO_2 uptake storage from 0.38 mmol g^{-1} (pristine GA) to 0.99 mmol g^{-1} (ZIF-8@GA) because of the synergistic effect between ZIF-8 and GA, which ranked this ZIF-8@GA among the most promising CO_2 adsorption materials. In addition, the mechanical robustness of ZIF-8@GA could be improved with the increased amount of ZIF-8 in the GA [81].

By synthesizing UiO-66 over a polyurethane foam template, Pinto et al. prepared UiO-66@polyurethane foam with a pore volume of $0.213 \text{ cm}^3 \text{ g}^{-1}$ and a BET surface area of $511 \text{ m}^2 \text{ g}^{-1}$. The UiO-66@polyurethane foam had exhibited more than 70% of adsorption capacity for n-hexane and benzene vapors. Besides, this composite presented good transport properties because UiO-66@polyurethane foam maintained the flexibility and macrostruc-

ture of the polyurethane foam, and can be used for gas adsorption [114].

These reports are the preliminary exploration of MOF-based aerogels in the field of gas adsorption. In this era of rapid economic development, new houses or decorated houses contain many harmful gases, such as formaldehyde, toluene, ethylbenzene, xylene, and so on [125,174,175]. Therefore, more kinds of MOF-based aerogels should be developed to adsorb these common harmful gases in the air to reduce their damage to the human body.

4.2.5. Sensing

Similar to the MOF-based hydrogels mentioned above for sensing, some aerogels also have sensing applications.

Zhao, Li and their research group have been devoted to the research and the development of MOF-based aerogels and their research on antibiotics and explosives sensing properties for a long time. This research group reported a water-stable Tb (III)-based metal-organic gel (MOG) [101]. After drying, the corresponding green aerogel was obtained with water stability and luminescence properties. The strong emission of the aerogel can be quenched via using trace amounts of sulfamethazine (SMZ) and sulfadiazine (SDZ). The aerogel exhibited sensitive detection ability effectively towards SMZ and SDZ with low detection limits of 0.086 and 0.218 ppm, respectively. Besides, the aerogel showed its application as a chemical sensor to detect explosive nitroaromatics, including 2,4-dinitrophenol (2,4-DNT) and 2,6-dinitrophenol (2,6-DNT). The aerogel exhibited sensitive detection ability effectively towards 2,4-DNT and (2,6-DNT) with low detection limits of 1.115 and 1.589 ppm, respectively.

They also designed a fluorescent MOG by metal-ion exchange between Eu^{3+} and Al^{3+} in the nonfluorescent MOG (Al) gel [102]. The corresponding red MOG (Eu) aerogel showed excellent sensing ability to ronidazole (RDZ), ornidazole (ODZ), metronidazole (MDZ), dimetridazole (DTZ), and 4-nitrophenol (4-NP). The corresponding limits were 1.205, 0.542, 0.999, 0.377, and 1.582 ppm, respectively. In addition, the selectivity and reversibility of the sensitive material were excellent. Therefore, the aerogel materials designed by Zhao, Li and their research group can combine sensitivity, selectivity and reversibility together in the detection of antibiotics and explosives, and are very promising in practical application.

Furthermore, some special MOF-based aerogels can also be employed in the fields of oil and water separation [176,177], electromagnetic pollution adsorption [89], electron adsorption, drug extraction [80], hydrocarbons separation [77], heavy-metal ions detection [178], and so on. These applications are fragmented and not systematic enough.

5. Conclusions and outlook

In summary, the categories and applications of MOF-based hydrogels and aerogels were reviewed detailly. MOF-based hydrogels and aerogels have received wide attention because of their outstanding flexible, structural, and chemical properties although the class of MOF-based hydrogels and aerogels is just an ordinary member of MOF materials family. The reported works have demonstrated the enhancements of processability and handling as well as environmental resistances as compared to MOF powders. This suggests that MOF-based hydrogels and aerogels could be adopted for practical applications in many areas, where MOF powders are not stable. This review provides a generalization of the cutting-edge development of the categories and applications of MOF-based hydrogels and aerogels by summarizing a great number of reported studies of MOF-based hydrogels and aerogels.

Although MOF-based hydrogels and aerogels had attracted increasing attention recently, this research area has not yet entered the mature stage. The stability of MOFs in MOF-based hydrogels and aerogels is key point that has been addressed owing to the fragility of MOFs during the processing conditions. MOFs in hydrogels and aerogels should retain high surface area, ordered structure and accessibility. Thus, these materials must be characterized by X-ray diffraction (XRD) and nitrogen isothermal adsorption measurements to confirm their stability after combined with hydrogel and aerogel matrixes.

In terms of the hydrogel and aerogel matrixes for constructing MOF-based hydrogels and aerogels, the examples of pure MOF hydrogels, MOF@biology derived organic macromolecules hydrogels, MOF@biocompatible hydrogels, MOF@ graphene hydrogels, pure MOF aerogels, MOF@silica aerogel composites, MOF@ graphene aerogel composites, MOF@cellulose aerogel composites, aerogel composites containing MOFs-derived materials, etc, are presented. All of these composites and their synthesizing strategies are used in preparing various MOF-based hydrogels and aerogels successfully, which widen the road for the rational optimization of MOFs with the enhancement of stabilization, accessibility, easy handling and flexibility for expanding the field of potential applications. Besides, these synthesizing strategies provide guidance for the synthesis of other MOF-based hydrogels and aerogels derived from unexplored MOFs. However, these strategies of synthesizing MOF-based hydrogels and aerogels are overly dependent on a limited variety of aerogel matrix materials. So, further exploration of widening the range of green and novel matrixes and advanced pure MOF hydrogels and aerogels is highly desirable.

Based on the advantages of rich porosity and structural flexibility as well as stability, scientists have made great efforts to explore versatile potential applications of MOF-based hydrogels and aerogels, including drug control release, wound healing, sensing, energy storage, catalysis, water treatment, gas adsorption, oil/water separation, electromagnetic pollution adsorption, electron absorption, drug extraction, hydrocarbons separation and so on. Even though these studies cover a wide range of the applications of MOF-based hydrogels and aerogels, the distribution of the applications is not balanced. Most applications are focused on electrochemistry, catalysis, and water treatment now. Besides, the studies on the practical applications of MOF-based hydrogels and aerogels still lack in depth and systematization. MOF-based hydrogels and aerogels are still at early stage compared with other MOF composites such as enzyme-MOF composites and metal nanoparticles-MOF composites. Consequently, more in-depth researches are needed to extend the applied range of MOF-based hydrogels and aerogels.

The large size and pipelined synthesis process of MOF-based hydrogels and aerogels with satisfactory stability implies their significant potential in industrial production, but some economical and green methods for synthesizing matrixes of MOF-based hydrogels and aerogels should be developed with repeatable quality, like naturally KMG aerogel. Once the economical MOF-based hydrogels and aerogels are implemented in large quantities to the industrially practical application level, it is a qualitative leap in the development of MOF materials. We hope that chemical and material researchers can be inspired by this review to come up with novel and smart ideas to stimulate the emergence of new materials and applications in the field of MOF-based hydrogels and aerogels. The diversity of MOFs and matrixes in MOF-based hydrogels and aerogels and their versatility offer unlimited possibilities for the regulation of the applied properties of this kind of materials. Therefore, these materials have great potential to achieve wider application in the future.

Acknowledgements

This work was supported by the National Natural Science Foundation of China, China (51602301 and 51672251), Science Foundation of Zhejiang Sci-Tech University, China (ZSTU) under Grant No. 13012138-Y and the Fundamental Research Funds of Zhejiang Sci-Tech University, China (2019Q007). Q. Z. acknowledges financial support from AcRF Tier 1, Singapore (RG 111/17, RG 2/17, RG 113/18) and Tier 2 (MOE 2017-T2-1-021 and MOE 2018-T2-1-070), Singapore. Q. Z. also thanks the funding support from State Key Laboratory of Supramolecular Structure and Materials, Jilin University, P. R. China (sklssm2019036). H. X. thanks the support from the Natural Science Foundation of Zhejiang Province, China (No. LY19E020007)

References

- [1] L.J. Murray, M. Dincă, J.R. Long, *Chem. Soc. Rev.* 38 (2009) 1294–1314.
- [2] T. Drake, P. Ji, W. Lin, *Accounts Chem. Res.* 51 (2018) 2129–2138.
- [3] X. Zhao, Y. Wang, D.S. Li, X. Bu, P. Feng, *Adv. Mater.* 30 (2018) 1705189.
- [4] Y. Cui, J. Zhang, H. He, G. Qian, *Chem. Soc. Rev.* 47 (2018) 5740–5785.
- [5] H.-C. Zhou, S. Kitagawa, *Chem. Soc. Rev.* 43 (2014) 5415–5418.
- [6] H. Wang, Q.-L. Zhu, R. Zou, Q. Xu, *Chem* 2 (2017) 52–80.
- [7] J. Cui, S. Ren, B. Sun, S. Jia, *Coord. Chem. Rev.* 370 (2018) 22–41.
- [8] M. Zhao, Y. Huang, Y. Peng, Z. Huang, Q. Ma, H. Zhang, *Chem. Soc. Rev.* 47 (2018) 6267–6295.
- [9] W. Lu, Z. Wei, Z.-Y. Gu, T.-F. Liu, J. Park, J. Park, J. Tian, M. Zhang, Q. Zhang, T. Gentle III, M. Bosch, H.-C. Zhou, *Chem. Soc. Rev.* 43 (2014) 5561–5593.
- [10] A.R. Kaija, C.E. Wilmer, *J. Phys. Chem. Lett.* 9 (2018) 4275–4281.
- [11] Y. He, B. Li, M. O’Keeffe, B. Chen, *Chem. Soc. Rev.* 43 (2014) 5618–5656.
- [12] A. Schoedel, M. Li, D. Li, M. O’Keeffe, O.M. Yaghi, *Chem. Rev.* 116 (2016) 12466–12535.
- [13] H.-L. Jiang, T.A. Makal, H.-C. Zhou, *Coord. Chem. Rev.* 257 (2013) 2232–2249.
- [14] D.-Y. Du, J.-S. Qin, S.-L. Li, Z.-M. Su, Y.-Q. Lan, *Chem. Soc. Rev.* 43 (2014) 4615–4632.
- [15] (a) J. Zhao, X. Liu, Y. Wu, D.-S. Li, Q. Zhang, *Coord. Chem. Rev.* 391 (2019) 30–43; (b) P. Li, F.-F. Cheng, W.-W. Xiong, Q. Zhang, *Inorg. Chem. Front.* 5 (2018) 2693; (c) J. Gao, M. He, Z.Y. Lee, W. Cao, W.-W. Xiong, Y. Li, R. Ganguly, T. Wu, Q. Zhang, *Dalton Trans.* 42 (2013) 11367–11370; (d) Y.-P. Wu, X.-Q. Wu, J.-F. Wang, J. Zhao, W.-W. Dong, D.-S. Li, Q. Zhang, *Crystal Growth Design* 16 (2016) 2309–2316; (e) G.-W. Xu, Y.-P. Wu, W.-W. Dong, J. Zhao, X.-Q. Wu, D.-S. Li, Q. Zhang, *Small* 13 (2017) 1602996.
- [16] Q.-L. Zhu, Q. Xu, *Chem. Soc. Rev.* 43 (2014) 5468–5512.
- [17] Q. Yang, Q. Xu, H.-L. Jiang, *Chem. Soc. Rev.* 46 (2017) 4774–4808.
- [18] N.S. Bobbitt, M.L. Mendonca, A.J. Howarth, T. Islamoglu, J.T. Hupp, O.K. Farha, R.Q. Snurr, *Chem. Soc. Rev.* 46 (2017) 3357–3385.
- [19] D.-S. Li, Y.-P. Wu, J. Zhao, J. Zhang, J.Y. Lu, *Coord. Chem. Rev.* 261 (2014) 1–27.
- [20] Y.P. Wu, W. Zhou, J. Zhao, W.W. Dong, Y.Q. Lan, D.S. Li, C. Sun, X. Bu, *Angew. Chem. Int. Ed.* 56 (2017) 13001–13005.
- [21] W. Zhou, D.-D. Huang, Y.-P. Wu, J. Zhao, T. Wu, J. Zhang, D.-S. Li, C. Sun, P. Feng, X. Bu, *Angew. Chem. Int. Ed.* 58 (2019) 4227–4231.
- [22] X.-K. Wang, J. Liu, L. Zhang, L.-Z. Dong, S.-L. Li, Y.-H. Kan, D.-S. Li, Y.-Q. Lan, *ACS Catal.* 9 (2019) 1726–1732.
- [23] F. Hiroyasu, K.E. Cordova, O.K. Michael, O.M. Yaghi, *Cheminform* 341 (2013) 974.
- [24] W. Lu, Y. Han, F. Xiao, J. Zhou, P. Qi, W. Bo, *Coord. Chem. Rev.* 307 (2016) 361–381.
- [25] C. Sun, C. Qin, C. Wang, Z. Su, S. Wang, X. Wang, G. Yang, K. Shao, Y. Lan, E. Wang, *Adv. Mater.* 23 (2011) 5629–5632.
- [26] J.-R. Li, J. Sculley, H.-C. Zhou, *Chem. Rev.* 112 (2011) 869–932.
- [27] J. Duan, W. Jin, S. Kitagawa, *Coord. Chem. Rev.* 332 (2017) 48–74.
- [28] H. Furukawa, K.E. Cordova, M. O’Keeffe, O.M. Yaghi, *Science* 341 (2013) 1230444.
- [29] Y. Cui, B. Chen, G. Qian, *Coord. Chem. Rev.* 273 (2014) 76–86.
- [30] Y. He, W. Zhou, G. Qian, B. Chen, *Chem. Soc. Rev.* 43 (2014) 5657–5678.
- [31] C. Li, H. Xu, J. Gao, W. Du, L. Shanguan, X. Zhang, R.-B. Lin, H. Wu, W. Zhou, X. Liu, J. Yao, B. Chen, *J. Mater. Chem. A* 7 (2019) 11928–11933.
- [32] Y. Li, M. Lu, Y. Wu, H. Xu, J. Gao, J. Yao, *Adv. Mater. Interfaces* 6 (2019) 1900290.
- [33] Y. Chen, S. Li, X. Pei, J. Zhou, X. Feng, S. Zhang, Y. Cheng, H. Li, R. Han, B. Wang, *Angew. Chem. Int. Ed.* 55 (2016) 3419–3423.
- [34] P. Neves, A.C. Gomes, T.R. Amarante, F.A.A. Paz, M. Pillinger, I.S. Gonçalves, A. A. Valente, *Micropor. Mesopor. Mater.* 202 (2015) 106–114.
- [35] G. Maurin, C. Serre, A. Cooper, G. Férey, *Chem. Soc. Rev.* 46 (2017) 3104–3107.
- [36] M. Carmen, L. Fátima, P. Elsa Quartapelle, S. Irena, K. Stefan, G. Simona, M. Norberto, B. Elisa, J.A.R. Navarro, *J. Am. Chem. Soc.* 133 (2011) 11888.
- [37] W. Zhang, Y. Hu, J. Ge, H.-L. Jiang, S.-H. Yu, *J. Am. Chem. Soc.* 136 (2014) 16978–16981.
- [38] A.J. Howarth, Y. Liu, P. Li, Z. Li, T.C. Wang, J.T. Hupp, O.K. Farha, *Nat. Rev. Mater.* 1 (2016) 15018.
- [39] V. Chan, P. Zorlutuna, J.H. Jeong, H. Kong, R. Bashir, *Lab Chip* 10 (2010) 2062.
- [40] S. Ye, J. Feng, P. Wu, *J. Mater. Chem. A* 1 (2013) 3495–3502.
- [41] C.A. García-González, M. Alnaief, I. Smirnova, *Carbohydr. Polym.* 86 (2011) 1425–1438.
- [42] A.C. Pierre, G.M. Pajonk, *Chem. Rev.* 34 (2002) 4243–4265.
- [43] S.S. Kistler, *Nature* 127 (1931), 741–741.
- [44] S.S. Kistler, *J. Phys. Chem.* 36 (1931) 52–64.
- [45] A. Kumar, A. Rana, G. Sharma, S. Sharma, M. Naushad, G.T. Mola, P. Dhiman, F. J. Stadler, *Environ. Chem. Lett.* (2018) 1–24.
- [46] K.J.D. France, T. Hoare, E.D. Cranston, *Chem. Mater.* 29 (2017) 4609–4631.
- [47] A. Schneemann, V. Bon, I. Schwedler, I. Senkovska, S. Kaskel, R.A. Fischer, *Chem. Soc. Rev.* 43 (2014) 6062–6096.
- [48] H. Liu, H. Peng, Y. Xin, J. Zhang, *Polym. Chem.* 10 (2019) 2263–2272.
- [49] F. Chen, Y.M. Wang, W. Guo, X.B. Yin, *Chem. Sci.* 10 (2019) 1644–1650.
- [50] A. Garai, W. Shepherd, J. Huo, D. Bradshaw, *J. Mater. Chem. B* 1 (2013) 3678.
- [51] S. Ren, C. Li, Z. Tan, Y. Hou, S. Jia, J. Cui, *J. Agri. Food. Chem.* 67 (2019) 3372.
- [52] N. Gao, J. Huang, L. Wang, J. Feng, P. Huang, F. Wu, *Appl. Surf. Sci.* 459 (2018) 686–692.
- [53] H. Zhu, Q. Zhang, S. Zhu, *ACS Appl. Mater. Inter.* 8 (2016) 17395–17401.
- [54] Y. Yu, G. Chen, J. Guo, Y. Liu, J. Ren, T. Kong, Y. Zhao, *Mater. Horiz.* 5 (2018) 1137–1142.
- [55] R. Ananthoji, J.F. Eubank, F. Nouar, H. Mouttaki, M. Eddaoudi, J.P. Harmon, *J. Mater. Chem.* 21 (2011) 9587–9594.
- [56] W.H. Chen, W.C. Liao, Y.S. Sohn, M. Fadeev, A. Cecconello, R. Nechushtai, I. Willner, *Adv. Funct. Mater.* 28 (2018) 1705137.
- [57] J. Xiao, S. Chen, J. Yi, H.F. Zhang, G.A. Ameer, *Adv. Funct. Mater.* 27 (2017) 1604872.
- [58] J.H. Lee, S. Kang, J. Jaworski, K.Y. Kwon, M.L. Seo, J.Y. Lee, J.H. Jung, *Chem. Eur. J.* 18 (2012) 765–769.
- [59] P. Huang, L.-F. Yan, *Chinese J. Chem. Phys.* 29 (2016) 742–748.
- [60] A. Chakraborty, P. Sutar, P. Yadav, M. Eswaramoorthy, T.K. Maji, *Inorg. Chem.* 57 (2018) 14480–14483.
- [61] Q. Zhu, Y. Li, W. Wang, G. Sun, K. Yan, D. Wang, *Compos. Commun.* 10 (2018) 36–40.
- [62] X. Lian, B. Yan, *Chem. Commun.* 55 (2019) 241–244.
- [63] Y. Zhuang, Y. Kong, X. Wang, B. Shi, *New J. Chem.* 43 (2019) 7202–7208.
- [64] O. Maan, P. Song, N. Chen, Q. Lu, *Adv. Mater. Interfaces* 6 (2019) 1801895.
- [65] M.S. Hoque, S. Benjakul, T. Prodpran, *Food Hydrocolloid.* 25 (2011) 1085–1097.
- [66] J. Yao, R. Chen, K. Wang, H. Wang, *Micropor. Mesopor. Mat.* 165 (2013) 200–204.
- [67] K. Deligkaris, T.S. Tadele, W. Olthuis, A. van den Berg, *Sensor. Actuat. B-Chem.* 147 (2010) 765–774.
- [68] X. Huang, Z. Yin, S. Wu, X. Qi, Q. He, Q. Zhang, Q. Yan, F. Boey, H. Zhang, *Small* 7 (2011) 1876–1902.
- [69] M.J. Allen, V.C. Tung, R.B. Kaner, *Chem. Rev.* 110 (2009) 132.
- [70] N. Stefania, C. Daniel, F.M. Luisa, M.C. Gutiérrez, D.M. Francisco, *Chem. Soc. Rev.* 42 (2013) 794–830.
- [71] S. Haiyan, X. Zhen, G. Chao, *Adv. Mater.* 25 (2013) 2554–2560.
- [72] M.R. Lohe, M. Rose, S. Kaskel, *Chem. Commun.* 2009 (2009) 6056–6058.
- [73] S. Xiang, L. Lei, J. Zhang, T. Xin, H. Cui, J. Shi, Y. Hu, L. Chen, C.Y. Su, S.L. James, *J. Mater. Chem.* 22 (2012) 1862–1867.
- [74] L. Li, S. Xiang, S. Cao, J. Zhang, G. Ouyang, L. Chen, C.Y. Su, *Nat. Commun.* 4 (2013) 1774.
- [75] B. Bueken, V.N. Van, T. Willhammar, T. Stassin, I. Stassen, D.A. Keen, G.V. Baron, D. Jfm, R. Ameloot, S. Bals, *Chem. Sci.* 8 (2017) 3939.
- [76] Z. Ulker, I. Erucar, S. Keskin, C. Erkey, *Micropor. Mesopor. Mat.* 170 (2013) 352–358.
- [77] A.L. Nuzhdin, A. Shalygin, E. Artiukha, A. Chibiryaev, G.A. Bukhtiyarova, O.N. Martyanov, *RSC Adv.* 6 (2016) 62501–62507.
- [78] A.S. Shalygin, A.L. Nuzhdin, G.A. Bukhtiyarova, O.N. Martyanov, *J. Sol-Gel Sci. Techn.* 84 (2017) 446–452.
- [79] A. Prabhu, A.A. Shoaibi, C. Srinivasakannan, *Mater. Lett.* 146 (2015) 43–46.
- [80] X. Zhang, Q. Liang, Q. Han, W. Wan, M. Ding, *Analyst* 141 (2016) 4219–4226.
- [81] M. Jiang, H. Li, L. Zhou, R. Xing, J. Zhang, *ACS Appl. Mater. Int.* 10 (2018) 827.
- [82] J. Mao, Y. Tang, Y. Wang, J. Huang, X. Dong, Z. Chen, Y. Lai, *iScience* 16 (2019) 133–144.
- [83] L. Lin, Y. Yang, Z. Cai, S. Lin, X. Hu, *Adv. Mater. Interfaces* (2018) 1701548.
- [84] J. Qu, D. Chen, N. Li, Q. Xu, H. Li, J. He, J. Lu, *Small* 14 (2018) 1800343.
- [85] J. Mao, M. Ge, J. Huang, Y. Lai, Y. Tang, *J. Mater. Chem. A* 5 (2017) 11873–11881.
- [86] Y. Xie, X. Tu, X. Ma, M. Xiao, G. Liu, F. Qu, R. Dai, L. Lu, W. Wang, *Electrochim. Acta* 311 (2019) 114–122.
- [87] H. Zhu, X. Yang, E.D. Cranston, S. Zhu, *Adv. Mater.* 28 (2016) 7652–7657.
- [88] W. Ren, J. Gao, C. Lei, Y. Xie, Y. Cai, Q. Ni, J. Yao, *Chem. Eng. J.* 349 (2018) 766–774.
- [89] X. Sun, X. Lv, M. Sui, X. Weng, X. Li, J. Wang, *Materials* 11 (2018) 781.
- [90] T. Jiang, F. Bu, X. Feng, I. Shakir, G. Hao, Y. Xu, *ACS Nano* 11 (2017) 5140–5147.
- [91] X. Xu, W. Shi, P. Li, S. Ye, C. Ye, H. Ye, T. Lu, A. Zheng, J. Zhu, L. Xu, M. Zhong, X. Cao, *Chem. Mater.* 29 (2017) 6058–6065.
- [92] Z. Liang, W. Xia, C. Qu, B. Qiu, H. Tabassum, S. Gao, R. Zou, *Chemelectrochem* 4 (2017) 2442–2447.
- [93] W. Xia, C. Qu, Z. Liang, B. Zhao, S. Dai, B. Qiu, Y. Jiao, Q. Zhang, X. Huang, W. Guo, D. Dang, R. Zou, D. Xia, Q. Xu, M. Liu, *Nano Lett.* 17 (2017) 2788–2795.

- [94] Z. Zhu, Y. Yang, Y. Guan, J. Xue, L. Cui, J. Mater. Chem. A 4 (2016) 15536–15545.
- [95] M. Wang, J. Zhang, H. Fan, B. Liu, J. Wang, New. J. Chem. 43 (2019) 5666–5669.
- [96] W. Zhang, S. Shi, W. Zhu, L. Huang, J. Wang, A.C.S. Sustain. Chem. Eng. 5 (2017) 9347–9354.
- [97] V. Ramasubbu, S. Alwin, E.M. Mothi, X.S. Shajan, Mater. Lett. 197 (2017) 236–240.
- [98] S. Alwin, V. Ramasubbu, X.S. Shajan, Bull. Mater. Sci. 41 (2018).
- [99] Y. Yuan, D. Yang, G. Mei, X. Hong, J. Wu, J. Zheng, J. Pang, Z. Yan, Colloid. Surface A 544 (2018) 187–195.
- [100] W. Yang, Y. Han, C. Li, L. Zhu, L. Shi, W. Tang, J. Wang, T. Yue, Z. Li, Chem. Eng. J. 375 (2019) 122076.
- [101] Z.-S. Qin, W.-W. Dong, J. Zhao, Y.-P. Wu, Q. Zhang, D.-S. Li, Inorg. Chem. Front. 5 (2018) 120–126.
- [102] Z.-S. Qin, W.-W. Dong, J. Zhao, Y.-P. Wu, Z.-F. Tian, Q. Zhang, D.-S. Li, Eur. J. Inorg. Chem. (2018) 186–193.
- [103] Y. Chen, X. Huang, S. Zhang, S. Li, S. Cao, X. Pei, J. Zhou, X. Feng, B. Wang, J. Am. Chem. Soc. 138 (2016) 10810–10813.
- [104] P. Jin, W. Tan, J. Huo, T. Liu, Y. Liang, S. Wang, D. Bradshaw, J. Mater. Chem. A 6 (2018) 20473–20479.
- [105] L. Chen, X. Ding, J. Huo, S. El Hankari, D. Bradshaw, J. Mater. Sci. 54 (2019) 370–382.
- [106] R. Ameloot, A. Liekens, L. Alaerts, M. Maes, A. Galarneau, B. Coq, G. Desmet, B. F. Sels, J.F.M. Denayer, D.E. De Vos, Eur. J. Inorg. Chem. 2010 (2010) 3735–3738.
- [107] X. Yan, X. Hu, S. Komarneni, RSC Adv. 4 (2014) 57501–57504.
- [108] H. Han, Z. Zongbin, W. Wubo, G. Yury, Q. Jieshan, Adv. Mater. 25 (2013) 2219–2223.
- [109] P. Hou, G. Xing, D. Han, Y. Zhao, G. Zhang, H. Wang, C. Zhao, C. Yu, J. Porous Mat. (2019) 1–12.
- [110] Z.L. Yu, B. Qin, Z.Y. Ma, J. Huang, S.C. Li, H.Y. Zhao, H. Li, Y.B. Zhu, H.A. Wu, S.H. Yu, Adv. Mater. (2019) 1900651.
- [111] R.J. Moon, M. Ashlie, N. John, S. John, Y. Jeff, Chem. Soc. Rev. 40 (2011) 3941–3994.
- [112] Y. Xuan, E.D. Cranston, Chem. Mater. 26 (2014) 6016–6025.
- [113] X. Cao, C. Tan, M. Sindoro, H. Zhang, Chem. Soc. Rev. 46 (2018) 2660.
- [114] M.L. Pinto, S. Dias, J. Pires, ACS Appl. Mater. Inter. 5 (2013) 2360–2363.
- [115] Z. Li, L. Yin, J. Mater. Chem. A 3 (2015) 21569–21577.
- [116] Z. He, Z. Qi, B.G. Li, S. Zhu, Z. He, Z. Qi, B.G. Li, S. Zhu, Z. He, Z. Qi, Adv. Mater. Inter. 4 (2017) 1700560.
- [117] J. Dong, Z. Hu, Y. Tong, J. Wang, M. Zhu, T. Chen, A. Yuan, Chem. Eng. J. 313 (2016) 1623–1632.
- [118] X. Cao, B. Zheng, X. Rui, W. Shi, Q. Yan, H. Zhang, Angew. Chem. Int. Ed. 126 (2014) 1428–1433.
- [119] N. Kamaly, B. Yameen, J. Wu, O.C. Farokhzad, Chem. Rev. 116 (2016) 2602–2663.
- [120] T.R. Dargaville, B.L. Farrugia, J.A. Broadbent, S. Pace, Z. Upton, N.H. Voelcker, Biosens. Bioelectron. 41 (2013) 30–42.
- [121] A. Gopal, V. Kant, A. Gopalakrishnan, S.K. Tandan, D. Kumar, Eur. J. Pharmacol. 731 (2014) 8–19.
- [122] L. Wang, J. Xu, X. Wang, Z. Cheng, J. Xu, Sensor. Actuat. B-Chem. 288 (2019) 289–297.
- [123] J. Zhao, Y.-N. Wang, W.-W. Dong, Y.-P. Wu, D.-S. Li, Q.-C. Zhang, Inorg. Chem. 55 (2016) 3265–3271.
- [124] Y. Zhang, S. Yuan, G. Day, X. Wang, X. Yang, H.-C. Zhou, Coord. Chem. Rev. 354 (2018) 28–45.
- [125] L. Wang, Y. Zhu, Q. Xiang, Z. Cheng, Y. Chen, J. Xu, Sensor. Actuat. B-Chem. 251 (2017) 590–600.
- [126] R.T. Kwok, C.W. Leung, J.W. Lam, B.Z. Tang, Chem. Soc. Rev. 44 (2015) 4228–4238.
- [127] H. Xu, J. Gao, X. Qian, J. Wang, H. He, Y. Cui, Y. Yang, Z. Wang, G. Qian, J. Mater. Chem. A 4 (2016) 10900–10905.
- [128] S. Sanda, S. Parshamoni, S. Biswas, S. Konar, Chem. Commun. 51 (2015) 6576–6579.
- [129] L.E. Kreno, K. Leong, O.K. Farha, M. Allendorf, R.P. Van Duyne, J.T. Hupp, Chem. Rev. 112 (2011) 1105–1125.
- [130] R. Finch, BMJ-Brit. Med. J. 300 (1990) 1289.
- [131] C. Bisson, N.B. Adams, B. Stevenson, A.A. Brindley, D. Polyviou, T.S. Bibby, P.J. Baker, C.N. Hunter, A. Hitchcock, Nat. Commun. 8 (2017) 1746.
- [132] G. Matafonova, V. Batoev, Water Res. 132 (2018) 177–189.
- [133] Y.G. Guo, J.S. Hu, L.J. Wan, Adv. Mater. 20 (2008) 2878–2887.
- [134] (a) Z. Qifeng, U. Evan, S.L. Candelaria, C. Guozhong, Chem. Soc. Rev. 42 (2013) 3127–3171;
(b) Z. Wu, J. Xie, Z. J. Xu, S. Zhang, Q. Zhang, J. Mater. Chem. A 7 (2019) 4259–4290;
(c) J. Xie, Z. Wang, Z.J. Xu, Q. Zhang, Adv. Energy Mater. 8 (2018) 1703509;
(d) Z.-Q. Lin, J. Xie, B. Zhang, J. Li, J.-N. Weng, R.-B. Song, X. Huang, H. Zhang, H. Li, Y. Liu, Z. J. Xu, W. Huang, Q. Zhang, Nano Energy 41 (2017) 117–127;
(e) J. Xie, P. Gu, Q. Zhang, ACS Energy Lett. 2 (2017) 1985–1996;
(f) J. Xie, Q. Zhang, J. Mater. Chem. A 4 (2016) 7091–7106;
(g) J. Xie, C.-E. Zhao, Z. Lin, P. Gu, Q. Zhang, Chem. Asian J. 11 (2016) 1489–1511;
(h) J. Wu, X. Rui, C. Wang, W.-B. Pei, R. Lau, Q. Yan, Q. Zhang, Adv. Energy Mater. 5 (2015) 1402189.
- [135] (a) M.V. Reddy, G.V. Rao, Subba, B.V.R. Chowdari, Chem. Rev. 113 (2013) 5364–5457;
(b) S. Wang, C. Sun, N. Wang, Q. Zhang, J. Mater. Chem. A 7 (2019) 10138–10158.
- [136] J. Shao, J. Feng, H. Zho, A. Yuan, Appl. Surf. Sci. 471 (2019) 745–752.
- [137] X. Ma, Y. Lou, X.-B. Chen, Z. Shi, Y. Xu, Chem. Eng. J. 356 (2019) 227–235.
- [138] D. Qu, J. Power Sources 109 (2002) 403–411.
- [139] S. Yuanlong, M.F. El-Kady, S. Jingyu, L. Yaogang, Z. Qinghong, Z. Meifang, W. Hongzhi, D. Bruce, R.B. Kaner, Chem. Rev. 118 (2018) 9233–9280.
- [140] L. Zhang, F. Zhang, X. Yang, G. Long, Y. Wu, T. Zhang, K. Leng, Y. Huang, Y. Ma, A. Yu, Sci. Rep. 3 (2013) 1408.
- [141] Q. Chong, Z. Lei, M. Wei, Z. Liang, B. Zhu, D. Dai, S. Dai, B. Zhao, H. Tabassum, G. Song, J. Mater. Chem. A 6 (2018) 4003–4012.
- [142] F. David, A. Sonia, P. Catherine, Angew. Chem. Int. Ed. 48 (2009) 7502–7513.
- [143] C. Kyung Min, N. Kyungsu, G.A. Somorjai, O.M. Yaghi, J. Am. Chem. Soc. 137 (2015) 7810–7816.
- [144] S. Jin, H.A. Gasteiger, N. Yabuuchi, H. Nakanishi, J.B. Goodenough, S.H. Yang, Nat. Chem. 3 (2011) 647.
- [145] L. Demarconnay, C. Coutanceau, J.M. Léger, Electrochim. Acta 49 (2004) 4513–4521.
- [146] H.C. Zhu, M. Chen, K. Li, X. Huang, F. Wang, ChemElectroChem 5 (2018) 2126–2134.
- [147] C. Li, B. Zhang, Y. Li, S. Hao, X. Cao, G. Yang, J. Wu, Y. Huang, Appl. Catal. B-Environ. 244 (2019) 56–62.
- [148] M. Escudero-Escribano, K.D. Jensen, A.W. Jensen, Curr. Opin. Electrochem. 8 (2018) 135–146.
- [149] J. Liu, L. Chen, H. Cui, J. Zhang, L. Zhang, C.Y. Su, Chem. Soc. Rev. 43 (2014) 6011–6061.
- [150] N. Huang, H. Drake, J. Li, J. Pang, Y. Wang, S. Yuan, Q. Wang, P. Cai, J. Qin, H.C. Zhou, Angew. Chem. Int. Ed. 57 (2018) 8916–8920.
- [151] R. Das, C.D. Vecitis, A. Schulze, B. Cao, A.F. Ismail, X. Lu, J. Chen, S. Ramakrishna, Chem. Soc. Rev. 46 (2017) 6946–7020.
- [152] A. Hu, X. Zhang, D. Luong, K. Oakes, M. Servos, R. Liang, S. Kurdi, P. Peng, Y. Zhou, Waste Biomass Valori. 3 (2012) 443–449.
- [153] A. Roy, A.K. Srivastava, B. Singh, D. Shah, T.H. Mahato, A. Srivastava, Dalton Trans. 41 (2012) 12346–12348.
- [154] H. Zhao, C. Ying, Q. Peng, Q. Wang, G. Zhao, Appl. Catal. B-Environ. 203 (2017) 127–137.
- [155] M.A. Barakat, Arab. J. Chem. 4 (2011) 361–377.
- [156] H. Gulyas, Water Sci. Technol. 36 (1997) 9–16.
- [157] G.P. Anipsitakis, D.D. Dionysiou, Appl. Catal. B-Environ. 54 (2004) 155–163.
- [158] J. Hu, G. Chen, I.M.C. Lo, Water Res. 39 (2005) 4528–4536.
- [159] S. Lang, Am. J. Ind. Med. 17 (2010) 189–214.
- [160] S. Bo, W. Ren, C. Lei, Y. Xie, Y. Cai, S. Wang, J. Gao, Q. Ni, J. Yao, J. Solid State Chem. 262 (2018) 135–141.
- [161] C. Lei, J. Gao, W. Ren, Y. Xie, S.Y.H. Abdalkarim, S. Wang, Q. Ni, J. Yao, Carbohydr. Polym. 205 (2019) 35–41.
- [162] K. Byrappa, A.K. Subramani, S. Ananda, K.M.L. Rai, R. Dinesh, M. Yoshimura, Bull. Mater. Sci. 29 (2006) 433–438.
- [163] P. Kumar, M. Govindaraju, S. Senthamilselvi, K. Premkumar, Colloid. Surface. B 103 (2013) 658–661.
- [164] V.K. Garg, R. Kumar, R. Gupta, Dyes Pigments 62 (2004) 1–10.
- [165] R. Ahmad, J. Hazard. Mater. 171 (2009) 767–773.
- [166] R. Ahmad, R. Kumar, Appl. Surf. Sci. 257 (2010) 1628–1633.
- [167] L. Zhu, L. Zong, X. Wu, M. Li, H. Wang, J. You, C. Li, ACS Nano 12 (2018) 4462–4468.
- [168] P. Hou, G. Xing, D. Han, H. Wang, C. Yu, Y. Li, J. Solid State Chem. 265 (2018) 184–192.
- [169] Q. Yang, R. Lu, S. Ren, C. Chen, Z. Chen, X. Yang, Chem. Eng. J. 348 (2018) 202–211.
- [170] K.-Y.A. Lin, H.-A. Chang, J. Mater. Chem. A 3 (2015) 20060–20064.
- [171] G. Li, S. Pang, Y. Wu, J. Ouyang, Chem. Eng. Commun. 205 (2018) 698–705.
- [172] S. Ma, M. Zhang, J. Nie, J. Tan, S. Song, Y. Luo, Carbohydr. Polym. 208 (2019) 328–335.
- [173] F. Cherubini, G.P. Peters, T. Berntsen, A.H. Stromman, E. Hertwich, GCB Bioenergy 3 (2011) 413–426.
- [174] X. Fang, L. Wang, X. He, J. Xu, Z. Duan, Inorg. Chem. 57 (2018) 1689–1692.
- [175] M. Horstjann, Y. Bakhrirkin, A. Kosterev, R. Curl, F. Tittel, C. Wong, C. Hill, R. Yang, Appl. Phys. B-Lasers O 79 (2004) 799–803.
- [176] S. Eom, D.W. Kang, M. Kang, J.H. Choe, C.S. Hong, Chem. Sci. 10 (2019) 2663–2669.
- [177] F. Zhang, L. Liu, X. Tan, X. Sang, J. Zhang, C. Liu, B. Zhang, B. Han, G. Yang, Soft Matter 13 (2017) 7365.
- [178] M. Lu, Y. Deng, Y. Luo, J. Lv, T. Li, J. Xu, S.-W. Chen, J. Wang, Anal. Chem. 91 (2019) 888–895.